OPTIMIZATION OF POINT ABSORBER DESIGN IN OCEAN WAVE ENERGY

A Thesis
Presented to
The Academic Faculty

By

Taylor McKie

Georgia Institute of Technology
August 2017

OPTIMIZATION OF POINT ABSORBER DESIGN IN OCEAN WAVE ENERGY

Approved by:

Dr. Kevin Haas, Advisor
School of Civil and Environmental Engineering
Georgia Institute of Technology

Dr. Hermann Fritz
School of Civil and Environmental Engineering
Georgia Institute of Technology

Date Approved: August 3rd, 2017

ACKNOWLEDGEMENTS

TABLE OF CONTENTS

Page

LIST OF TABLES

LIST OF FIGURES

LIST OF SYMBOLS AND ABBREVIATIONS

A	Added Mass
B	Radiation Damping Coefficient
C_g	Group Velocity
D	Float Diameter
E	Energy
η	Efficiency
F	Force
f	Frequency
g	Gravity
H	Wave Height
h	Water Depth
k	Wave Number
m	Mass
ω	Wave Frequency
P	Power
$\Re$	Real
ρ	Density
T	Period
t	Time
V	Volume
$\dot{x}$	Velocity
$\ddot{x}$	Acceleration

ABSTRACT

The purpose of this study is to analyze the factors that affect the efficiency of a wave energy conversion device and design an optimal point absorber float geometry considering the various factors. Factors to be analyzed in the study include damping system design, resonance, float geometry, and the kinematics of the device. This study will utilize Fusion 360, Nemoh, and Wec-Sim to achieve the objectives. Fusion 360 will be used to design point absorber float geometries. Nemoh will be used to simulate the hydrodynamic response of each float design. Wec-Sim will be used to vary the wave conditions and calculate the efficiencies of the various designs based off of the response generated in Nemoh. From this, trends will be observed and an optimal geometry can be determined. The results of this study can be used to further optimize point absorber systems and provide solutions to minimize the difficulty of extracting energy from ocean waves.

CHAPTER 1

INTRODUCTION

With climate change and its detrimental effect on the environment, there is a need to not only implement the use of more known renewable energy sources, such as solar and wind, but also to expand our knowledge of other renewables. Ocean wave energy, a centuries old idea, has become more prevalent over the past few decades because of its ability to travel long distances with little energy loss, ability to sustain power availability 90% of the time, and its wide availability in multiple locations (Lopez, 2013). Despite the fact that there are already many conversion devices utilized in the field, wave energy presents many challenges. The conversion of oscillatory motions of waves into useful electricity, the varying power levels, thus inconsistent efficiencies due to the varying periods of irregular wave patterns, and the alignment of a conversion device to capture the most energy possible with dynamic wave directions represent a few of these challenges (Lopez et al., 2013). Given these challenges, the current objective in researching wave energy extraction and conversion devices involves developing methods and mechanisms for optimal efficiency.

Various types of wave energy converters have evolved, resulting in different ways in which wave energy can be absorbed. Falcão (2010) categorizes conversion devices by oscillating water columns, oscillating bodies, and overtopping devices. Oscillating bodies includes single body heaving systems, two-body heaving systems, fully submerged heaving systems, pitching devices, bottom hinged systems, and multi-body systems. Devices may also possess other names but contain the same function. Lopez et al.

classifies conversion devices by attenuators, point absorbers, and terminators. For the purpose of this study, a combination of the concepts behind these devices may be appropriate, but the focus will be on point absorbers as a single body heaving system.

Point absorbers respond to the heaving movement of the waves, extracting the energy from the waves mechanically through its linear power take-off system (PTO). The translator, attached to the float, and the stator, attached to the spare and plate, moves relative to each other, thus allowing the generation of electricity. Figure 1 illustrates the point absorber system. Various factors influence the efficiency of the point absorber device, including its float geometry, damping within the power take-off system, size, and center of gravity.
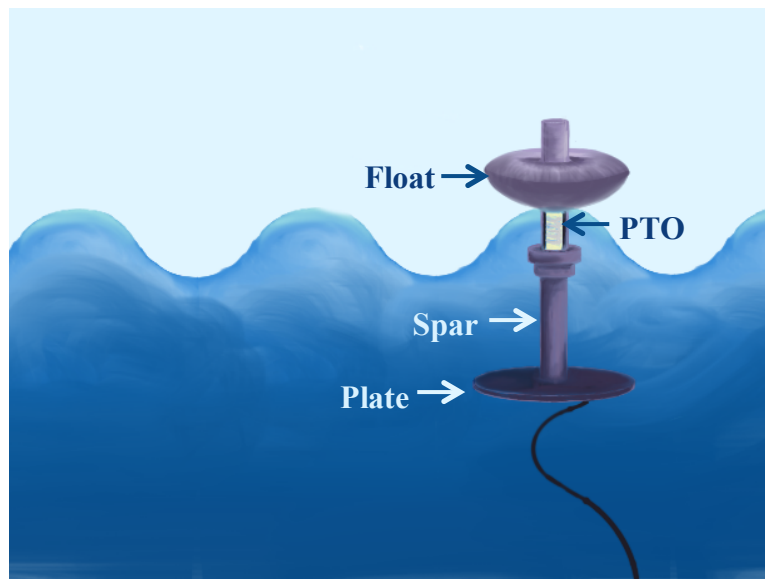
Figure 1. Point absorber wave energy conversion system
(Waves are not to scale)

Because irregular waves vary in period and force distribution, it is difficult to effectively convert the wave energy into a usable form; therefore, considering these factors becomes crucial. The studies of Salter (1974) and Banasiak et al. (2004) observe

the influence of the geometry of a point absorber on the overall efficiency of the design. Banasiak et al. (2004) tested various geometries, finding that hemispherical and conical (with a 90° pointed angle) shapes are the most efficient designs with a constant damping coefficient. Though Salter (1974) rejected the idea of a heaving device, his design of the pitching device, or "Duck", considered the circular pattern of waves with hopes that the design would capture a concatenated force from the dispersed and random wave forces.

Another factor to consider in optimizing point absorber devices is the resonance condition. Falcão (2013) discussed the significance of resonance, proposing that wave energy conversion devices should operate as dynamic systems, instead of quasi-static systems. Resonance occurs when the float velocity is in phase with the excitation forces of the waves that act on the wetted surface. It is with this behavior that the device will be most efficient. The factors of the design, including the float geometry, system damping, size, mass, and center of gravity may relate to this phenomenon of resonance. This study will examine these relationships and attempt to achieve optimal results, as there is a lack of research related to the geometric design and its relation to the efficiency of the system.

This study will examine the relationship between geometry, damping, and mass in regular and irregular waves under the consideration of the concept of resonance theory. It will also explore and recommend different approaches in analyzing irregular ocean waves and their relationship to resonance as well as optimal design considerations. Finally, this study will utilize modeling and simulation tools including Nemoh, BEMIO, and WEC-Sim to model and test the various designs presented and these results will be compared to the results in literature.

CHAPTER 2

METHODS

In order to achieve the objective of this study, various float geometries were designed in Fusion 360, simulated in Nemoh and BEMIO, and tested in WEC-Sim. This section will cover the methods and procedures of designing the floats, calculating the hydrodynamic coefficients using each simulation tool, analyzing a set of irregular waves, modeling the conversion devices, and calculating the efficiencies. A matrix of all test conditions will also be presented.

2.1   NUMERICAL MODEL DESCRIPTIONS

2.1.1   Nemoh

Nemoh is an open source boundary-element method code used to simulate the hydrodynamic response of each float (Babarit, 2015). The code computes first order wave loads on offshore structures. Each float created in Fusion 360 will be converted into an acceptable format for aximesh.m, a mesh generator, to create the mesh design, folder structure, and input files necessary to run Nemoh. The output files of Nemoh include solutions to the linear boundary value problems, radiation coefficients, diffraction coefficients, and excitation force values. The radiation coefficients describe the interaction and forces of the submerged body on the water without additional incident waves. This includes added mass and radiation damping. The diffraction coefficients describe the interactions of the various waves caused by radiation and excitation. These

4

outputs are required for calculations through the boundary element method involved in BEMIO.

2.1.2 BEMIO

BEMIO is a pre- and post-processing tool that reads in the outputs from Nemoh and generates a Hierarchical Data Format 5 file (.h5). In pre-processing, BEMIO calculates the radiation and excitation impulse response functions, calculates the state space realization coefficients from the hydrodynamic data Nemoh outputs. In post-processing, BEMIO saves and compiles all of the information from both Nemoh and BEMIO into the .h5 file, which is required to operate WEC-Sim.

2.1.3 WEC-Sim

WEC-Sim is an open-source wave energy converter (WEC) simulation tool that utilizes MATLAB and Simulink to model the relationship of the components of the device, such as the float and the power take-off system, and its response to the hydrodynamic motion of the waves in various conditions. WEC-Sim will output kinematics, forces, and pressures of the waves, float bodies, power take-off systems, and components of the system by solving the equation of motion for a wave energy conversion system (Yu, 2014). The output can then be analyzed in MATLAB for efficiency and other parameters.

2.2 METHODOLOGY

2.2.1 Designing the Floats

The float designs tested in this study included the default point absorber float design in WEC-Sim, Reference Model 3 (RM3) (Neary, 2014); the hemispherical, 60° conical, 90° conical, and 120° conical float designs suggested and studied by Banasiak et al. (2004); and an innovative float design based off an analysis of irregular waves. Each of the designs were modeled in Fusion 360, a product of Autodesk. The designs were then converted into a format acceptable for the input in Nemoh.

To create the floats within Fusion 360, the workspace was initially in MODEL mode. Using the tools under SKETCH, a 2-dimensional lateral profile of half the float design was created. Then using the Revolve tool under CREATE, the profile becomes a 3-dimensional body. Slight adjustments were then made to each body using the tools under MODIFY. To convert the model into .stl mesh format, the body was selected under BROWSER and Save As STL was selected.

In order to analyze the efficiency of the each system as a function of float geometry, the masses of each body needed to be the same. Assuming each body will consist of the same material, the volume of each body needed to be the same. To modify the size and adjust the volume of each body, Scale under MODIFY was selected and a percentage to increase or decrease the size was determined. To check the new volume of the body, the body was selected under BROWSER, and Properties was selected. The volume of each body was compared to that of RM3, so scaling each body became an iterative process until the volume of the body matched the volume of RM3. The same process was applied in creating the 500,000 kg and 1,000,000 kg floats.

The center of gravity was also needed as an input to aximesh.m in Nemoh. The center of gravity was found under Properties after selecting the body. Similarly, the mass

of the body was recorded from Properties. In order to position the body accurately in Nemoh, the displacement volume was calculated using the mass found under Properties. The displacement volume was calculated using
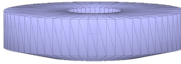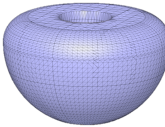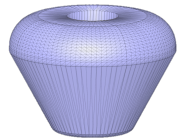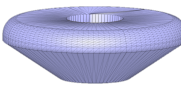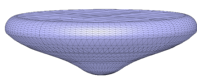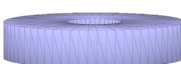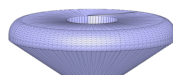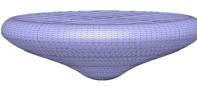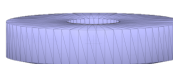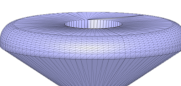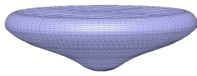
$$V_{disp} = \frac{m_{float}}{\rho_w} \qquad (1)$$

where V_{disp} is the displacement volume, m_{float} is the mass of the float, and ρ_w is the density of water. To find the location of the center of gravity for each float within Fusion 360, first the .stl file was opened in the MODEL workspace through INSERT by selecting Insert Mesh. Then the workspace was changed to MESH and under MODIFY, Plane Cut was selected. The Cut Type was changed to Trim and the Fill Type was changed to Uniform. The Y Angle was changed to 90.0 degrees to display only the bottom half of the body. After finalizing the plane cut, the workspace was changed to MODEL and Mesh to BRep was selected under the body in BROWSER. Selecting the body, the volume can be viewed by selecting Properties. This volume must match the displacement volume. If the volume does not equal the displacement volume, then the body must be returned to its original form and the process becomes iterative until the volume of the cut body equals the displacement volume. The displacement height was found by using the Measure tool under INSPECT by measuring the vertical height of the split body. Similarly, the height of the center of gravity from the bottom of the body was found. The properties of each float are defined in Table 1. Once the body size, displacement volume, center of mass was determined, the body was then converted manually into an acceptable form for to run aximesh.m in Nemoh.

To convert the body into an acceptable form for aximesh.m, the number of vertical vertices (n), radius corresponding to each horizontal circular profile of each vertex (r), and the vertical location of each vertex (z), needed to be found.

Table 1: Float Properties

	Mass [kg]	727,010		Mass [kg]	727,010
	Volume [m³]	1,298		Volume [m³]	1,302
	Diameter [m]	20		Diameter [m]	16.043
	Center of Mass	-0.735		Center of Mass	-0.6537
	Moment of Inertia, I_{xx} [m⁴]	2.86E+08		Moment of Inertia, I_{xx} [m⁴]	2.14E+08
	Moment of Inertia, I_{yy} [m⁴]	2.86E+08		Moment of Inertia, I_{yy} [m⁴]	2.14E+08
RM3	Moment of Inertia, I_{zz} [m⁴]	5.36E+08	**Hemisphere**	Moment of Inertia, I_{zz} [m⁴]	3.09E+08
	Mass [kg]	727,010		Mass [kg]	727,010
	Volume [m³]	1,298		Volume [m³]	1,296
	Diameter [m]	16.478		Diameter [m]	19.9
	Center of Mass	-0.789		Center of Mass	-0.613
	Moment of Inertia, I_{xx} [m⁴]	2.20E+08		Moment of Inertia, I_{xx} [m⁴]	2.56E+08
	Moment of Inertia, I_{yy} [m⁴]	2.20E+08		Moment of Inertia, I_{yy} [m⁴]	2.56E+08
60° Cone	Moment of Inertia, I_{zz} [m⁴]	3.00E+08	**90° Cone**	Moment of Inertia, I_{zz} [m⁴]	4.46E+08
	Mass [kg]	727,010		Mass [kg]	727,010
	Volume [m³]	1,293		Volume [m³]	1,298
	Diameter [m]	21.8		Diameter [m]	21.432
	Center of Mass	-0.412		Center of Mass	-0.397
	Moment of Inertia, I_{xx} [m⁴]	2.96E+08		Moment of Inertia, I_{xx} [m⁴]	2.53E+08
	Moment of Inertia, I_{yy} [m⁴]	2.96E+08		Moment of Inertia, I_{yy} [m⁴]	2.53E+08
120° Cone	Moment of Inertia, I_{zz} [m⁴]	5.52E+08	**Innovative**	Moment of Inertia, I_{zz} [m⁴]	4.70E+08
	Mass [kg]	500,000		Mass [kg]	500,000
	Volume [m³]	893		Volume [m³]	893
	Diameter [m]	17.636		Diameter [m]	19.272
	Center of Mass	-0.354		Center of Mass	-0.367
	Moment of Inertia, I_{xx} [m⁴]	1.54E+08		Moment of Inertia, I_{xx} [m⁴]	1.60E+08
	Moment of Inertia, I_{yy} [m⁴]	1.54E+08		Moment of Inertia, I_{yy} [m⁴]	1.60E+08
RM3	Moment of Inertia, I_{zz} [m⁴]	2.87E+08	**120° Cone**	Moment of Inertia, I_{zz} [m⁴]	2.98E+08
	Mass [kg]	500,000		Mass [kg]	1,000,000
	Volume [m³]	892		Volume [m³]	1,787
	Diameter [m]	18.913		Diameter [m]	22.248
	Center of Mass	-0.354		Center of Mass	-0.329
	Moment of Inertia, I_{xx} [m⁴]	1.35E+08		Moment of Inertia, I_{xx} [m⁴]	4.87E+08
	Moment of Inertia, I_{yy} [m⁴]	1.35E+08		Moment of Inertia, I_{yy} [m⁴]	4.87E+08
Innovative	Moment of Inertia, I_{zz} [m⁴]	2.52E+08	**RM3**	Moment of Inertia, I_{zz} [m⁴]	9.12E+08
	Mass [kg]	1,000,000		Mass [kg]	1,000,000
	Volume [m³]	1,782		Volume [m³]	1,786
	Diameter [m]	24.257		Diameter [m]	23.839
	Center of Mass	-0.471		Center of Mass	-0.416
	Moment of Inertia, I_{xx} [m⁴]	5.05E+08		Moment of Inertia, I_{xx} [m⁴]	4.31E+08
	Moment of Inertia, I_{yy} [m⁴]	5.05E+08		Moment of Inertia, I_{yy} [m⁴]	4.31E+08
120° Cone	Moment of Inertia, I_{zz} [m⁴]	9.42E+08	**Innovative**	Moment of Inertia, I_{zz} [m⁴]	8.01E+08

The displacement height of the body was set to z = 0, and the z value of the center of

mass was set to the distance between the location of the center of mass and the

displacement height. The radii were found by measuring the horizontal distance between

each horizontal pair of vertices, then dividing the value by 2. The corresponding z values

were found by measuring the vertical distance between the displacement height and the

vertices. These values were then arranged into vectors. In order to receive consistent

results with the geometric control variable, the same protocol was applied to RM3. The

original .stl file was inserted into Fusion 360 and the dimensions were measured. The

vectors for each of the geometries with a mass of 727,010 kg are displayed in Table 2.

For the geometries with a mass of 500,000 kg and 1,000,000 kg, the vectors are displayed

in Table 3. These vectors were then used as inputs for aximesh.m.

2.2.2   Calculation of Hydrodynamic Coefficients

Before using Nemoh, aximesh.m was used for mesh generation. The inputs for

aximesh include the n, r, and z vectors, number of discretization, number of panels, and

center of gravity. For all of the float designs, 72 points for angular discretization and 150

target panels were used. Aximesh.m outputs mesh files containing parameters of the

body and an identification file. The inputs for Nemoh include the outputs from

aximesh.m as well as an input text file and an input file describing the parameters of the

sea environment, description of the bodies and degrees of freedom, range and increments

of wave frequencies, and post processing information. For the trials in this study, the

wave frequencies range from 0.02 to 5.2 Hz in increments of 0.02 Hz, the wave direction

9

input was 0, and the water depth input was 0 for deep water. Running Nemoh involves running three programs: pre-processor, solver, and post-processor (Babarit, 2015).

Table 2: Aximesh Vectors for Float Geometries with Mass of 727,010 kg
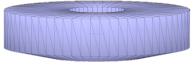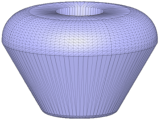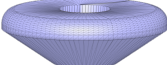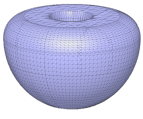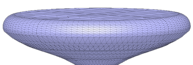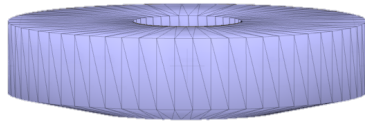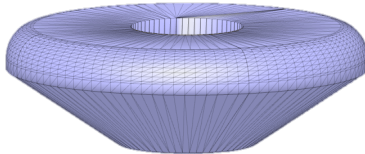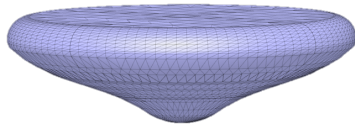
RM3			60° Cone			90° Cone			120° Cone			Hemisphere			Innovative		
n	r	z	n	r	z	n	r	z	n	r	z	n	r	z	n	r	z
4	10	1.989	16	5.891	3.429	16	8.235	2.096	15	9.435	1.779	36	6.49	3.423	35	9.426	1.438
	10	0		6.583	3.284		8.595	2.041		9.654	1.731		6.51	3.368		9.512	1.372
	10	-2.01		7.129	3.016		8.845	1.951		9.888	1.646		6.555	3.283		9.841	1.276
	5	-3.04		7.567	2.637		9.118	1.829		10.14	1.526		6.732	3.169		10.08	1.152
				7.906	2.165		9.326	1.677		10.33	1.374		6.965	3.027		10.26	1.003
				8.129	1.621		9.495	1.499		10.53	1.194		7.169	2.859		10.42	0.834
				8.226	1.03		9.647	1.299		10.66	0.989		7.38	2.667		10.54	0.649
				8.239	0.571		9.769	1.083		10.76	0.765		7.553	2.454		10.63	0.453
				8.147	0.159		9.859	0.855		10.85	0.526		7.702	2.223		10.7	0.251
				8.147	0		9.931	0.622		10.88	0.279		7.824	1.976		10.7	0.129
				7.691	-0.79		9.941	0.125		10.88	0.154		7.923	1.717		10.7	0
				4.071	-7.06		9.941	0		10.88	0		7.985	1.449		10.65	-0.15
				3.953	-7.18		4.737	-5.08		10.88	-0.39		8.017	1.176		10.58	-0.35
				3.829	-7.28		4.566	-5.19		4.195	-4.25		8.013	1.039		9.699	-0.79
				3.687	-7.36		4.347	-5.27		4.016	-4.31		8.016	0.792		9.067	-1.11
				3.5	-7.42		4.197	-5.31					7.986	0.299		7.982	-1.59
													7.943	0		7.725	-1.68
													7.918	-0.19		7.489	-1.76
													7.827	-0.67		6.52	-2.06
													7.707	-1.15		6.087	-2.19
													7.557	-1.62		5.167	-2.47
													7.386	-2.08		4.68	-2.62
													7.173	-2.53		4.305	-2.75
													6.946	-2.97		3.741	-2.96
													6.673	-3.39		2.655	-3.46
													6.394	-3.79		2.018	-3.82
													6.085	-4.18		1.815	-3.92
													5.753	-4.54		1.613	-4.01
													5.404	-4.88		1.422	-4.08
													5.028	-5.21		1.218	-4.14
													4.629	-5.5		1.007	-4.2
													4.222	-5.78		0.793	-4.24
													3.773	-6.02		0.571	-4.27
													3.32	-6.24		0.318	-4.3
													2.869	-6.44		0.15	-4.31
													2.511	-6.49			

Table 3: Aximesh Vectors for Float Geometries with Mass of 500,000 kg and 1,000,000 kg

RM3						120° Cone						Innovative					
500,000 kg			1,000,000 kg			500,000 kg			1,000,000 kg			500,000 kg			1,000,000 kg		
n	r	z	n	r	z	n	r	z	n	r	z	n	r	z	n	r	z
3	8.818	1.755	3	11.11	2.221	14	8.281	1.569	14	10.39	1.967	35	8	1.438	32	10.83	1.717
	8.818	-1.78		11.11	-2.23		8.566	1.527		10.71	1.914		8.394	1.372		11.06	1.634
	4.412	-2.69		5.558	-3.37		8.774	1.452		11	1.82		8.837	1.276		11.36	1.513
							8.977	1.346		11.28	1.687		9.045	1.152		11.6	1.168
							9.153	1.212		11.51	1.518		9.19	1.003		11.73	0.955
							9.306	1.053		11.69	1.317		9.292	0.834		11.84	0.722
							9.433	0.872		11.85	1.089		9.373	0.649		11.89	0.475
							9.531	0.674		12	0.839		9.397	0.453		11.91	0.221
							9.589	0.463		12.07	0.573		9.439	0.251		11.92	0.067
							9.623	0.244		12.12	0.298		9.457	0.129		11.79	-0.2
							9.636	0.133		12.11	0.159		9.399	0		10.79	-1
							9.636	-0.35		12.13	-0.45		9.334	-0.15		10.08	-1.42
							3.717	-3.76		4.668	-4.74		9.082	-0.35		8.871	-2.02
							3.591	-3.81		4.504	-4.81		8.559	-0.79		8.546	-2.12
													7.976	-1.11		8.349	-2.24
													6.984	-1.59		7.231	-2.61
													6.792	-1.68		6.753	-2.77
													6.583	-1.76		5.726	-3.12
													5.711	-2.06		5.173	-3.31
													5.321	-2.19		4.77	-3.46
													4.535	-2.47		4.123	-3.72
													4.122	-2.62		2.942	-4.35
													3.8	-2.75		2.227	-4.79
													3.302	-2.96		2.012	-4.91
													2.343	-3.46		1.804	-5.04
													1.781	-3.82		1.568	-5.14
													1.597	-3.92		1.351	-5.22
													1.426	-4.01		1.121	-5.29
													1.255	-4.08		0.883	-5.35
													1.072	-4.14		0.6	-5.39
													0.877	-4.2		0.343	-5.42
													0.7	-4.24		0.082	-5.43
													0.509	-4.27			
													0.32	-4.3			
													0.034	-4.31			

The pre-processor prepares the mesh and generates the conditions of each body for all of the calculation cases determined in the Nemoh input file. The Solver solves the linear boundary value problems and post-processor provides other parameters, such as added mass, radiation damping, and excitation force values. To solve for these values, the sum of the hydrodynamic forces, F_{HD} is assessed by

$$F_{HD} = A\ddot{x} + B\ddot{x} + F_D \qquad (2)$$

where A is the added mass, B is the radiation damping coefficient, F_D is the diffraction force, and $\ddot{x}$ is acceleration.

$$F_D = F_X + F_K = \int_{S_w} \frac{\partial(\phi_X + \phi_K)}{\partial t}\hat{n}ds \qquad (3)$$

expresses the diffraction forces in terms of velocity potential, where F_K is the wave diffraction force and F_X is the wave excitation force induced by wave diffraction (Li, 2012). Once these non-dimensionalized values were determined within Nemoh, the data was prepared for WEC-Sim through BEMIO. In running BEMIO, a structure was created and the function called the filename of the body and read the data stored from solver and the post-processing of Nemoh. BEMIO then calculated the normalized, excitation, and state space realization of the radiation impulse response functions and stored the read and calculated data into the structure. BEMIO then wrote the structure into an .h5 file for WEC-Sim.

2.2.3 Modeling the Wave Energy Converter

After the .h5 file was created in BEMIO, WEC-Sim imported the hydrodynamic coefficients and scaled the values defined by Yu (2014) as

12

$$\left|\overline{F_X(\omega)}\right| = \frac{|F_X(\omega)|}{\rho_w g} \qquad (4)$$

$$\left|\overline{A(\omega)}\right| = \frac{A(\omega)}{\rho_w} \qquad (5)$$

$$\left|\overline{B(\omega)}\right| = \frac{B(\omega)}{\rho_w \omega} \qquad (6)$$

$$\overline{F_K} = \frac{F_K}{\rho_w g} \qquad (7)$$

where ω is wave frequency and g is gravity. These values were incorporated into the equation for the dynamic response of the point absorber system under various conditions. The response of the system was modeled using

$$m\ddot{x} = F_E + F_R + F_{PTO} + F_V + F_{ME} + F_B + F_M \qquad (8)$$

where F_E is the wave excitation force, F_R is the radiation force, F_{PTO} is the power take-off force, F_V is the damping force, F_{ME} is the Morison Element Force, F_B is the buoyancy force, and F_M is the mooring connection force (Babarit, 2012).

The system response was subject to two assumptions for the wave conditions: monochromatic waves using the convolution integral equation and a user-defined spectrum using the Joint North Sea Wave Project Spectrum (JONSWAP). For regular waves, the radiation force was modeled in using

$$F_R = -A_\infty \ddot{x} - \int_0^t K(t - \tau)\dot{x}(\tau)d\tau \qquad (9)$$

and the excitation force was modeled using

$$F_E = \Re\left[R_f \frac{H}{2} F_X(\omega)e^{i(\omega t)}\right] \qquad (10)$$

where A_∞ is the added mass at infinite frequency, $\dot{x}$ is velocity, R_f is the ramp function for the wave simulation, H is wave height, and F_X is the excitation vector. Within the

13

WEC-Sim Input File, these functions were utilized by defining the variables under the commented section Regular Waves. The wave class was set to 'regularCIC' and the wave height in meters and wave period in seconds were defined. The JONSWAP Spectrum was used for testing how the system responded to irregular waves. For this condition, the parameters are displayed in Table 4.

Table 4: Assumptions for JONSWAP Spectrum

Frequency Interval df [1/s]	Maximum Frequency f_{max} [1/s]	Water Depth h [m]	Peak Period T_p [s]	Peak Factor	Significant Wave Height H [m]
1/100	0.5	200	6.5	$\{2, 5, 10, 20\}$	2.5

The peak period was chosen to be 6.5 seconds because the peak efficiency of each design in regular waves ranged from 6 to 7 seconds. The wave number, k, for each frequency was determined using the dispersion relationship expressed as

$$k = \frac{2\pi}{T\sqrt{gh}} - \left(\frac{\frac{4\pi^2}{T^2} - \frac{2\pi g}{T\sqrt{gh}} * \tanh\frac{2\pi h}{T\sqrt{gh}}}{-g\tanh\frac{2\pi h}{T\sqrt{gh}} - \frac{2\pi gh}{T\sqrt{gh}} * \left(\text{sech}\frac{2\pi h}{T\sqrt{gh}}\right)^2} \right) \quad (11)$$

where T is the wave period, and h is the water depth.

The JONSWAP Spectrum equations are expressed as

$$S^*(f) = \frac{g^2}{(2\pi)^4} f^{-5} e^{\left[-\frac{5}{4}\left(\frac{f_p}{f}\right)^4\right]} \gamma^\Gamma \quad (12)$$

$$\Gamma = e^{\left[-\left(\frac{\frac{f}{f_p}-1}{\sqrt{2}\sigma}\right)^2\right]}, \sigma = \begin{cases} 0.07 & f \leq f_p \\ 0.09 & f > f_p \end{cases} \quad (13)$$

$$\alpha_j = \frac{H_{m_o}^2}{16 \int_0^\infty S^*(f) df} \quad (14)$$

$$S(f) = \frac{\alpha_j g^2}{(2\pi)^4} f^{-5} e^{\left[-\frac{5}{4}\left(\frac{f_p}{f}\right)^4\right]} \gamma^{\Gamma} \qquad (15)$$

where γ^{Γ} is the peak enhancement factor, f_p is the peak frequency, $S(f)$ is the wave

spectra, and H_{m_o} is the significant wave height. The wave spectra and frequency vectors

were written to a text file. Within the WEC-Sim Input File, the irregular wave spectrum

was defined under the commented section Irregular Waves using User-Defined Spectrum.

The wave class was set to 'irregularImport' and the spectrum data file was set to the

name of the text file created from the JONSWAP calculations.

The system response was also dependent on various other factors that were

manipulated within the WEC-Sim Input File. These factors included the body data, spar

data, power take-off system data, and mooring connection. For the body, the body class

was changed to the directory of the .h5 file for each individual float design to read the

hydrodynamic data. The moment of inertia was also included as input as well as .stl file

for the geometry file for visualization. The spar from RM3 was used for all float designs

with the body class remaining in the same file directory as the RM3 .h5 file. The original

power take-off system and mooring connection for RM3 were used for all float designs.

After WEC-Sim was executed by typing wecSim in the MATLAB Command

Window, various matrices were outputted. The outputs included time series of the wave

elevation and responses from the body, power take-off, mooring connection, and

constraints in six degrees of freedom. This output was then manipulated and assessed for

analysis. A summary of the modeling process is depicted in Figure 2.
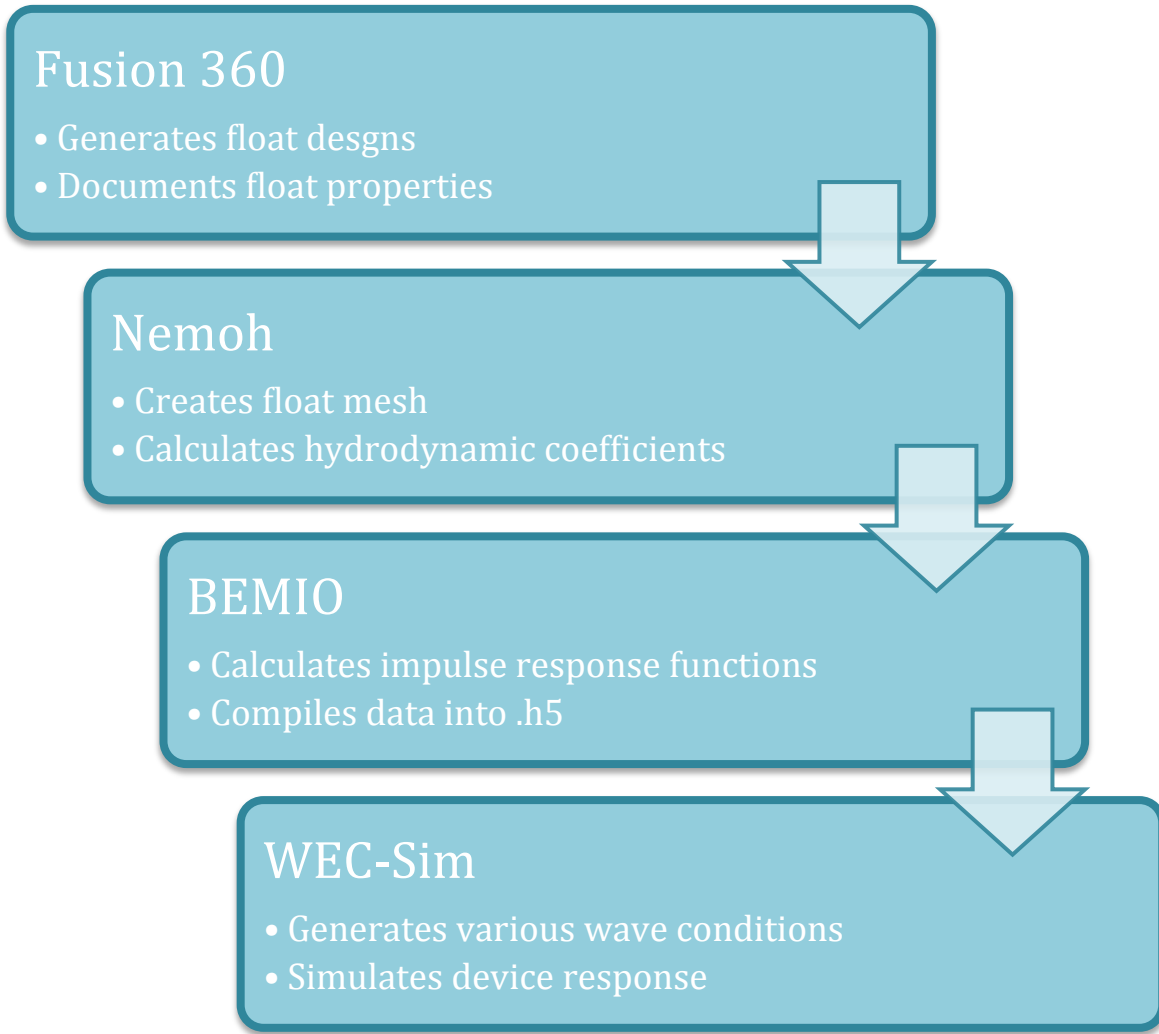
Figure 2. Flow chart of the modeling process for each point absorber design

2.2.4 Final Calculations

The power generated by the waves, P_{waves}, is calculated by

$$n = \frac{1}{2}\left(\frac{1 + 2kh}{\sinh 2kh}\right) \qquad (16)$$

$$C_g = \frac{2\pi n}{kT} \qquad (17)$$

$$P_{waves} = \frac{1}{16}\left(\frac{\rho_w g H^2 C_g D}{1000}\right) \qquad (18)$$

16

where n is used to compute the group velocity, C_g, based on the phase velocity, and D is the diameter of the float. The energy of the waves, E_{waves}, and power take-off system, E_{PTO}, are illustrated in Equations 19 and 20, respectively. The power take-off system response was retrieved from the heave column of the power take-off output structure.

$$E_{waves} = P_{waves}\Delta t \qquad (19)$$

$$E_{PTO} = \int_{t_o}^{t} P_{PTO}dt \qquad (20)$$

where Δt is the difference in time between the beginning and end of the simulation and dt was time step size. The efficiency of the system, η, was calculated using

$$\eta = \frac{E_{PTO}}{E_{waves}} * 100 \qquad (21)$$

2.3   TEST CONDITIONS

The trials for testing float design took place in two phases. Phase I tested the 6 float designs varying the wave conditions as illustrated in Table 5. Of the hemisphere and cone designs, the most efficient design with the given parameters will be tested in Phase 2 of the experiment. In Phase II, RM3, the optimal design from Phase I, and the Innovative Design will be tested varying the mass and damping coefficients as illustrated in Table 6.
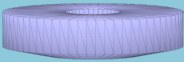
Table 5: Phase I Test Conditions for Float Design
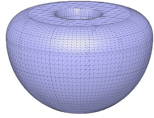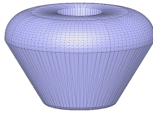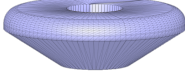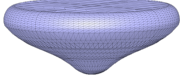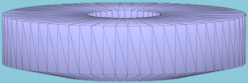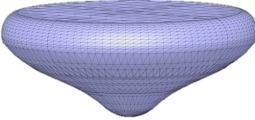
Control Geometry: RM3	Hemisphere	60° Cone	90° Cone	120° Cone	Innovative Design	Control Variables
Conditions	Regular Waves Wave Height (H) = {1, 1.5, 2, 2.5, 3, 3.5, 4} [m] Wave Period (T) = {4, 5, 6, 7, 8, 9, 10, 11, 12, 13, 14, 15, 16} [s]					Mass 727010 kg
	Irregular Waves Refer to **Table 4**					Damping 1200 kN/(m/s)

Table 6: Phase II Test Conditions for Float Design

	Control Geometry: RM3	Optimal Geometry	Innovative Design	Control Variables
Conditions	Mass {500000, 727010, 1000000} [kg]			Damping: 1200 kN/(m/s) Regular Wave Conditions Wave Height: H = 2.5 m Wave Period: [4 ≤ T ≤ 16] s Irregular Wave Conditions
	Damping {1200, 2500, 4800} [kN/(m/s)]			Mass: 727010 kg Regular Wave Conditions Wave Height: H = 2.5 m Wave Period: [4 ≤ T ≤ 16] s Irregular Wave Conditions

CHAPTER 3

RESULTS & DISCUSSION

This section will be comprised of the results from the irregular wave analysis that was used to create the innovative float design and the results from the trials of Phase I and Phase II. The results from Phase I will display the trends of the six float geometries in regular and irregular wave conditions. The results from Phase II will display the trends in mass and damping for RM3, the innovative design, and the most efficient design from Phase I.

3.1   IRREGULAR WAVE ANALYSIS

An analysis on the force distribution of irregular waves was performed in order to inspire an innovative approach to designing the float geometry of a point absorber. Resonance theory motivated this analysis, shifting the focus to how the shape of the device would cause a certain response in velocity due to the force distribution of the waves. In order to reduce the number of parameters for the analysis, dimensional analysis using the Buckingham Pi Theorem was used to find similitude. Three dimensionless parameters were used: the ratio of excitation force in surge to heave, $\frac{g}{H\omega^2}$, the ratio of the magnitude of the resultant force to the maximum force, and dimensionless time.

Irregular waves were defined in WEC-Sim with a peak period of 6.5 seconds and a peak factor of 2. The surge and heave components of the excitation force vectors of the resulting waves were extracted for 30 consecutive waves. Figure 3 illustrates the ratio of

the magnitudes of the heave and surge forces as a function of the non-dimensional

parameter determined from Buckingham Pi. A majority of the points demonstrated that

the forces in the surge direction were less than the heave and had similar ratios, although

no specific dependence on the non-dimensional parameter was found. The magnitude of

the differential resultant force was non-dimensionalized as a ratio to the maximum force

of each wave and is displayed as a function of non- dimensional time in Figure 4.
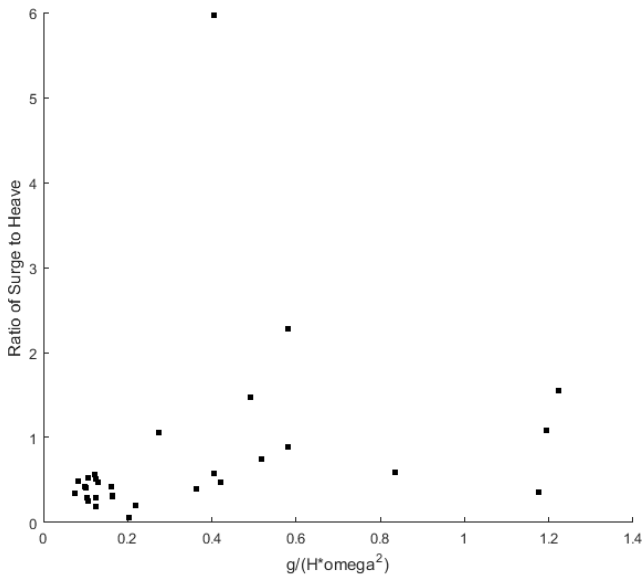
Figure 3. Ratio of the surge to heave forces as a function of non-dimensional wave height and frequency
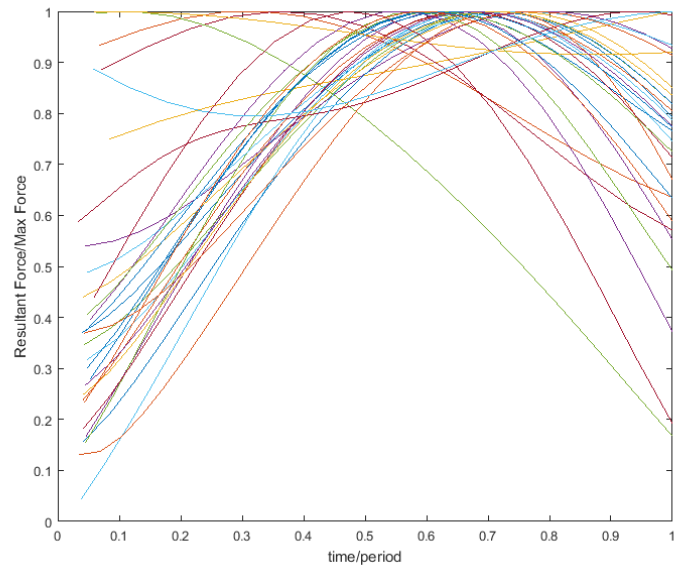
Figure 4. Ratio of the resultant force to the maximum force as a function of non-dimensional time

This relationship displayed great similitude between the irregular waves in terms of the

shape of the curve. Similarly, the angle of each differential resultant force was graphed

as a function of non-dimensional time in Figure 5. This also demonstrated similitude in

magnitude and shape. The general shape of these curves was used to determine the

geometry of the innovative float, displayed in Figure 6 and 7.
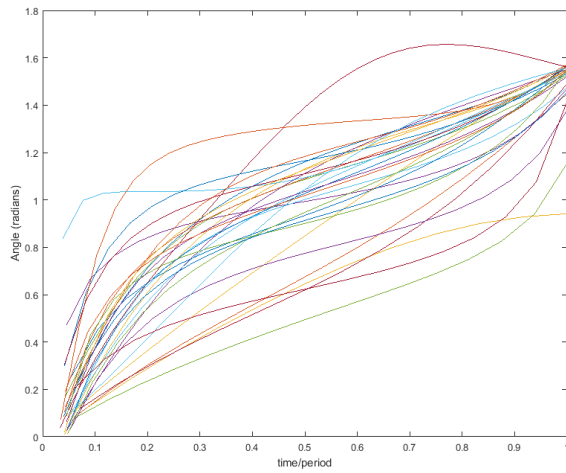
Figure 5. Angle of the differential resultant force as a function of non-dimensional time
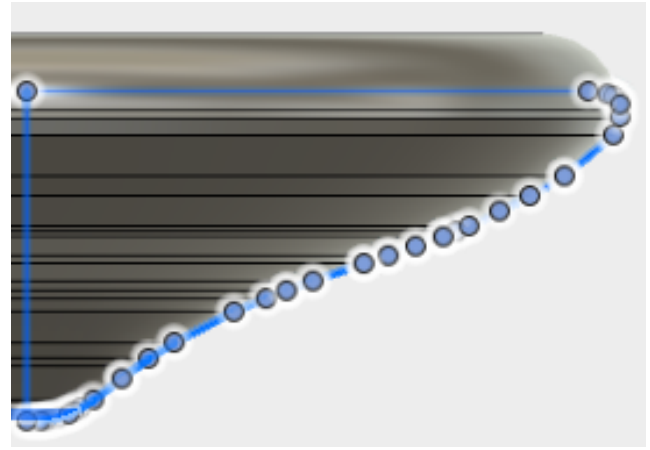
Figure 6. Profile of the innovative float design
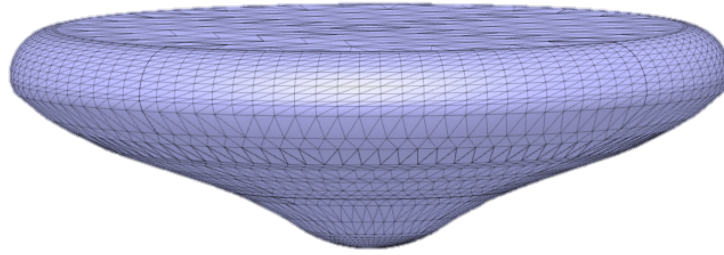
Figure 7. Innovative float design

There was a limitation in the design in which there was a lack of understanding in how the angle of each differential force could affect the kinematics of the surface. For this reason, the float geometry mirrors the trend in Figure 5.

3.2   PHASE I RESULTS

This section displays and discusses the results from the test conditions listed in Table 5. Phase I tested the six float geometries in regular and irregular wave conditions with constant mass and damping. Figure 8 displays the efficiencies for the hemispherical float geometry with varying wave period and wave height. Similarly, Figures 9, 10, and

21

11 display the efficiencies for the conical geometries with the 60°, 90°, and 120° angles, respectively. Figure 12 displays the efficiencies for the innovative geometry. Figure 13 displays the efficiencies for the control geometry, RM3. The maximum efficiency overall was 73.31% with the 120° conical float. Figure 14 compares the efficiency trends of the six float geometries as a function of wave period. The 120° cone, innovative, and RM3 designs were relatively more efficient for the period range of 5 to 9 seconds, with 120° cone being the most efficient. For periods greater than 9 seconds, the efficiencies of each float tend to be the same. This could imply that the geometry may only affect the performance of the float around the peak period of its resonant frequency, whereas beyond that range, mass may be more significant.

		Wave Period (s)												
		4	5	6	7	8	9	10	11	12	13	14	15	16
	1	21.32	40.07	51.86	52.97	45.99	35.86	26.25	18.56	11.82	9.05	6.37	4.49	3.23
	1.5	21.32	40.07	51.85	52.96	45.98	35.85	26.24	18.55	8.17	9.04	6.36	4.49	3.23
Wave Height (m)	2	21.32	40.07	51.85	52.96	45.97	35.84	26.23	18.55	6.23	9.03	6.36	4.48	3.23
	2.5	21.32	40.07	51.85	52.95	45.96	35.83	26.22	18.54	4.98	9.03	6.35	4.48	3.22
	3	21.32	40.07	51.84	52.94	45.95	35.82	26.21	18.53	4.14	9.02	6.34	4.47	3.22
	3.5	21.32	40.07	51.84	52.93	45.94	35.81	26.20	18.52	3.59	9.01	6.34	4.47	3.21
	4	21.32	40.07	51.84	52.93	45.93	35.79	26.18	18.51	3.26	9.01	6.33	4.46	3.21

Figure 8. Efficiencies for the hemispherical float geometry for regular waves as a function of wave period and wave height

Wave Period (s)

	4	5	6	7	8	9	10	11	12	13	14	15	16
1	23.48	39.09	48.09	48.81	42.40	33.43	24.64	17.59	12.44	8.73	6.16	4.38	3.17
1.5	23.48	39.09	48.09	48.80	42.39	33.42	24.63	17.58	11.77	8.73	6.15	4.37	3.17
2	23.48	39.08	48.08	48.79	42.38	33.41	24.62	17.57	9.59	8.72	6.14	4.37	3.16
2.5	23.48	39.08	48.08	48.78	42.37	33.40	24.61	17.56	7.88	8.71	6.14	4.36	3.16
3	23.48	39.08	48.07	48.77	42.36	33.39	24.60	17.55	6.57	8.70	6.13	4.36	3.15
3.5	23.48	39.08	48.07	48.77	42.35	33.37	24.59	17.54	5.60	8.70	6.12	4.35	3.15
4	23.48	39.08	48.07	48.76	42.33	33.36	24.58	17.53	4.90	8.70	6.12	4.34	3.14

(Wave Height (m) is the vertical axis label)

Figure 9. Efficiencies for the conical float geometry with the 60° angle for regular waves as a function of wave period and wave height

Wave Period (s)

	4	5	6	7	8	9	10	11	12	13	14	15	16
1	35.40	50.90	59.66	57.68	48.32	36.95	22.70	18.50	12.90	8.87	6.21	4.37	3.13
1.5	35.40	50.90	59.65	57.67	48.30	36.94	12.24	18.48	12.89	8.36	6.21	4.37	3.13
2	35.40	50.89	59.64	57.66	48.29	36.92	8.36	18.47	12.88	8.86	6.20	4.37	3.13
2.5	35.40	50.89	59.64	57.65	48.28	36.91	6.57	18.47	12.87	8.85	6.20	4.36	3.13
3	35.40	50.89	59.63	57.64	48.56	36.90	5.64	18.46	12.86	8.84	6.19	4.36	3.12
3.5	35.40	50.89	59.62	57.63	48.25	36.88	5.21	18.45	12.85	8.84	6.19	4.35	3.12
4	35.40	50.89	59.62	57.62	48.24	36.87	5.13	18.43	12.84	8.83	6.18	4.35	3.12

(Wave Height (m) is the vertical axis label)

Figure 10. Efficiencies for the conical float geometry with the 90° angle for regular waves as a function of wave period and wave height

Wave Period (s)

	4	5	6	7	8	9	10	11	12	13	14	15	16
1	38.30	62.88	73.31	72.50	57.86	43.15	29.34	20.18	13.77	9.52	6.42	4.54	3.29
1.5	38.30	62.88	73.30	72.48	57.85	43.14	25.86	20.17	13.76	9.51	6.42	4.54	3.29
2	38.30	62.88	73.29	72.47	57.83	43.12	21.46	20.16	13.75	9.51	6.41	4.53	3.28
2.5	38.30	62.87	73.29	72.46	57.82	43.10	18.29	20.14	13.74	9.50	6.41	4.53	3.28
3	38.30	62.87	73.28	72.44	57.80	43.09	15.82	20.13	13.74	9.49	6.40	4.53	3.28
3.5	38.30	62.87	73.27	72.43	57.78	43.07	13.94	20.13	13.73	9.48	6.39	4.52	3.27
4	38.29	62.87	73.27	72.42	57.77	43.06	12.53	20.12	13.72	9.47	6.39	4.52	3.27

(Wave Height (m) — vertical axis label)

Figure 11. Efficiencies for the conical float geometry with the 120° angle for regular waves as a function of wave period and wave height

Wave Period (s)

	4	5	6	7	8	9	10	11	12	13	14	15	16
1	40.59	59.18	67.14	62.97	51.43	38.27	27.10	18.64	12.81	8.75	6.11	4.27	3.05
1.5	40.59	59.18	67.13	62.96	51.42	38.26	27.09	18.63	12.80	8.75	6.10	4.27	3.05
2	40.59	59.17	67.13	62.95	51.41	38.24	27.08	18.62	12.79	8.74	6.10	4.26	3.05
2.5	40.59	59.17	67.12	62.93	51.40	38.23	27.07	18.61	12.79	8.74	6.10	4.26	3.05
3	40.59	59.17	67.11	62.92	51.38	38.23	27.06	18.60	12.78	8.73	6.09	4.26	3.05
3.5	40.59	59.17	67.11	62.91	51.37	37.86	27.05	18.59	12.77	8.73	6.09	4.26	3.05
4	40.59	59.16	67.10	62.90	51.36	35.71	27.04	18.58	12.76	8.72	6.08	4.26	3.05

(Wave Height (m) — vertical axis label)

Figure 12. Efficiencies for the innovative float geometry for regular waves as a function of wave period and wave height

	Wave Period (s)												
	4	5	6	7	8	9	10	11	12	13	14	15	16
1	33.74	60.23	71.40	62.33	51.80	39.03	29.09	19.59	13.79	9.17	6.65	4.61	3.21
1.5	33.74	60.23	71.39	62.31	51.78	39.01	29.07	19.58	13.78	9.17	6.64	4.61	3.21
2	33.74	60.22	71.39	62.30	51.77	39.00	29.06	19.57	13.77	9.16	6.63	4.60	3.21
2.5	33.73	60.22	71.38	62.29	51.75	38.98	29.04	19.56	13.76	9.15	6.63	4.60	3.21
3	33.73	60.22	71.38	62.28	51.74	38.97	29.03	19.55	13.75	9.15	6.62	4.59	3.21
3.5	33.72	60.22	71.37	62.27	51.72	38.97	15.22	19.54	13.74	9.14	6.62	4.59	3.20
4	33.72	60.22	71.37	62.26	51.71	39.01	5.79	19.53	13.72	9.13	6.61	4.58	3.20

(Wave Height (m) — row labels; Wave Period (s) — column headers)

Figure 13. Efficiencies for the control geometry, RM3, for regular waves as a function of wave period and wave height
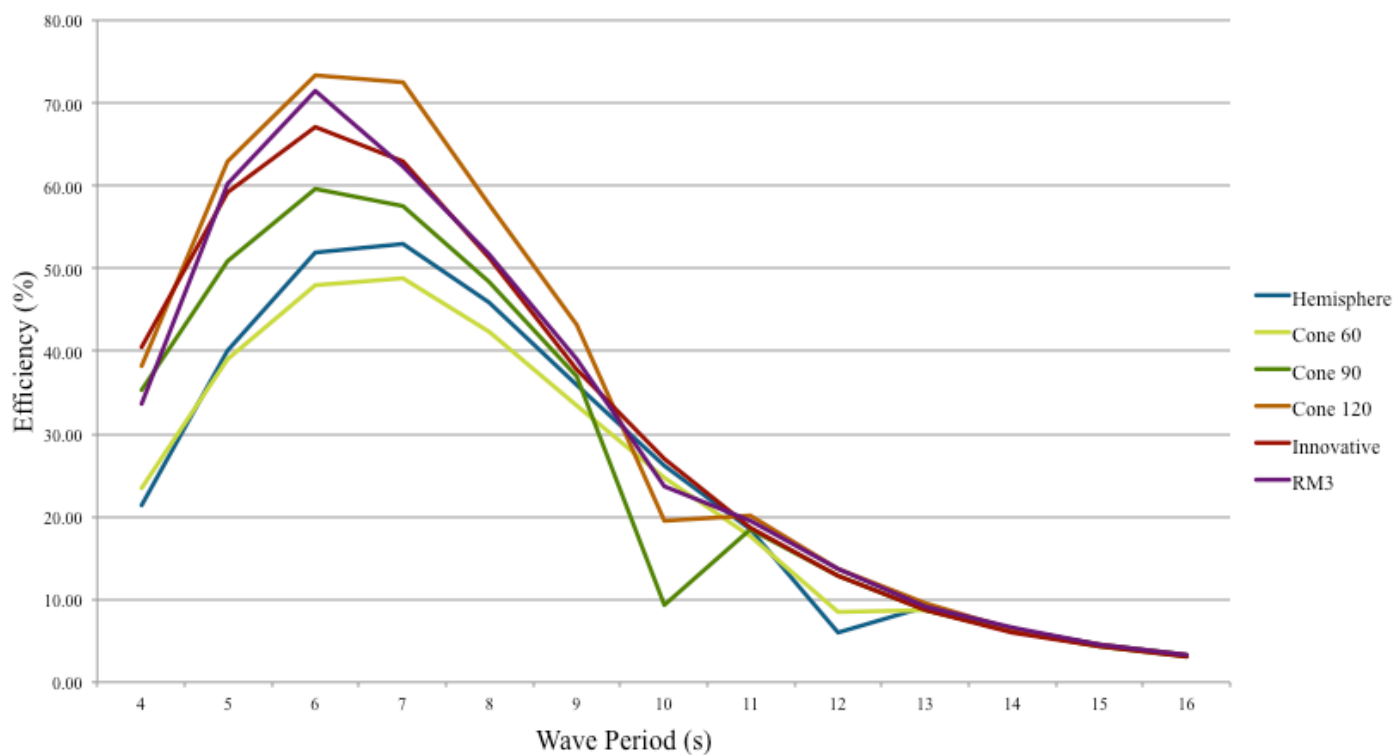

Figure 14. Efficiency as a function of wave period for the six float geometries at a wave height of 2.5m

25

Figure 15 illustrates the relative maximum efficiency for the six float geometries.

Because the 120° cone was the most efficient design, it was tested in Phase II for varying

mass and damping. For the irregular waves, efficiency was plotted as a function of peak

enhancement factor for all six designs as displayed in Figure 16. Generally, the

efficiency increases as a function of peak enhancement factor because of the lower

variation of wave periods associated with larger peak enhancement factors. Overall, the

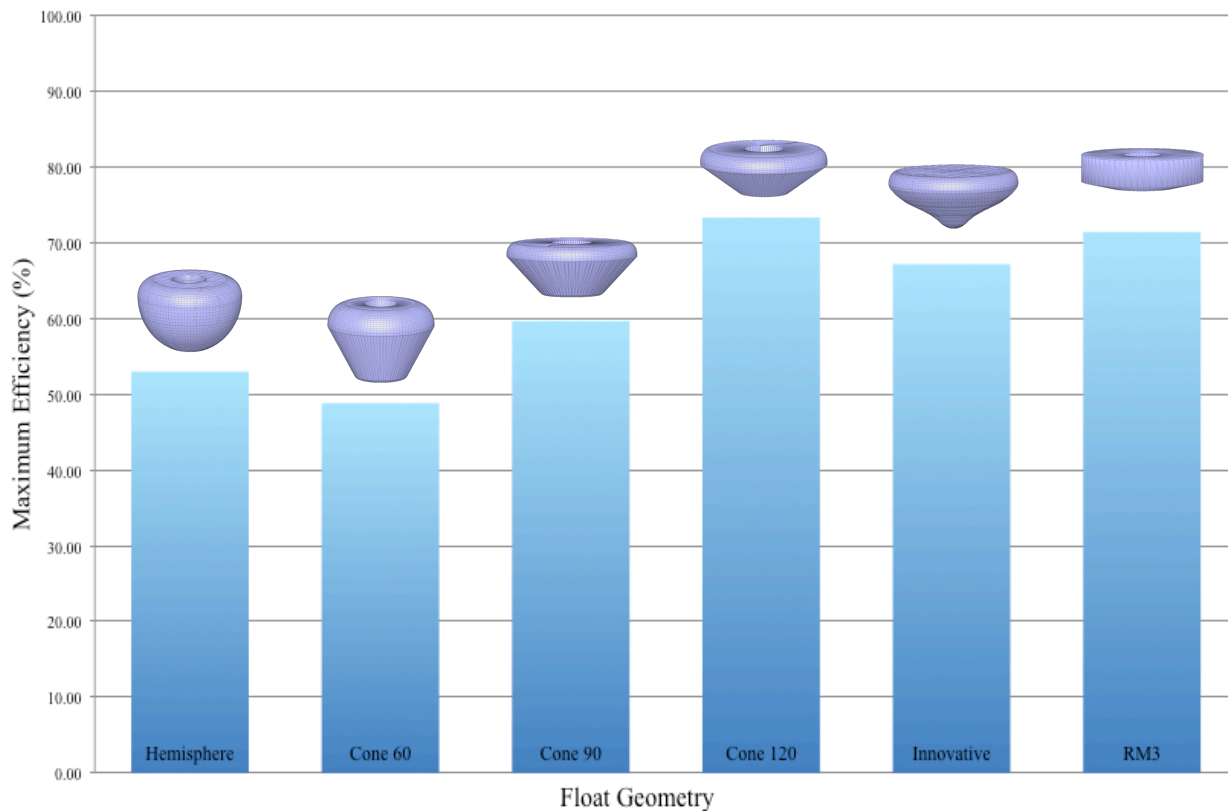120° cone was the most efficient with an average of 29.60% for the irregular wave trials.

Figure 15. Maximum efficiency[*] for the six float geometries in regular waves (At various periods (hemisphere and 60° cone at 7 seconds, remaining at 6 seconds))
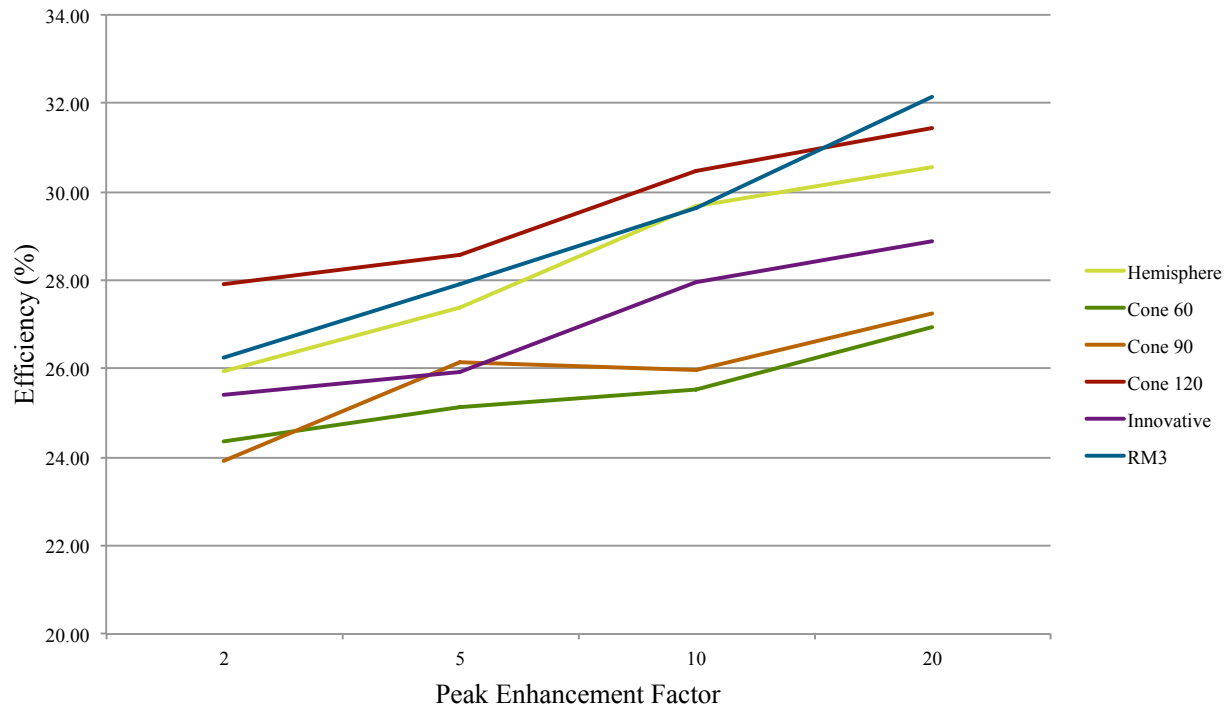
Figure 16. Efficiency as a function of peak enhancement factor for the six float geometries in irregular waves

3.3 PHASE II RESULTS

For Phase II, the 120° cone, innovative, RM3 designs were tested with the conditions displayed in Table 6. For the mass trials, damping was held constant. For regular waves, Figure 17 displays the efficiency of each float at a mass of 500,000 kg as a function of wave period. The 120° cone was the most efficient at a peak period of 7 seconds with an efficiency of 73.95%. This curve also shifted to the right in its peak period. Innovative and RM3 were approximately equal. RM3 and 120° cone were inconsistent in the trend at a period of 10 seconds for reasons undetermined. Figure 18 illustrates the efficiency of each float at a mass of 1,000,000 kg as a function of wave period. RM3 was the most efficient design with a peak efficiency of 73.53% at a period of 6 seconds. Figure 19 displays a summary of how each float compares in efficiency with varying mass by illustrating the maximum efficiency of each float at each mass in

regular waves. For innovative and 120° cone, the efficiency decreases as the mass

increases and for RM3, the efficiency increases as mass increases. This implies that the

efficiency of a float design depends on both the geometry and mass, as one mass value

may not complement every geometric design. For irregular waves, efficiency was plotted

as a function of peak enhancement factor for 500,000 kg and 1,000,000 kg in Figures 20

and 21, respectively. For a mass of 500,000 kg, 120° cone was the most efficient with an

average efficiency of 31.77%, followed by innovative, then RM3. Similarly, the

efficiency will increase as a function of peak enhancement factor for the reasons

aforementioned. For a mass of 1,000,000, RM3 was the most efficient overall with an

average efficiency of 29.09%, followed by 120° cone, then innovative. Figure 22

illustrates an overview of the irregular wave trials for mass with the maximum efficiency

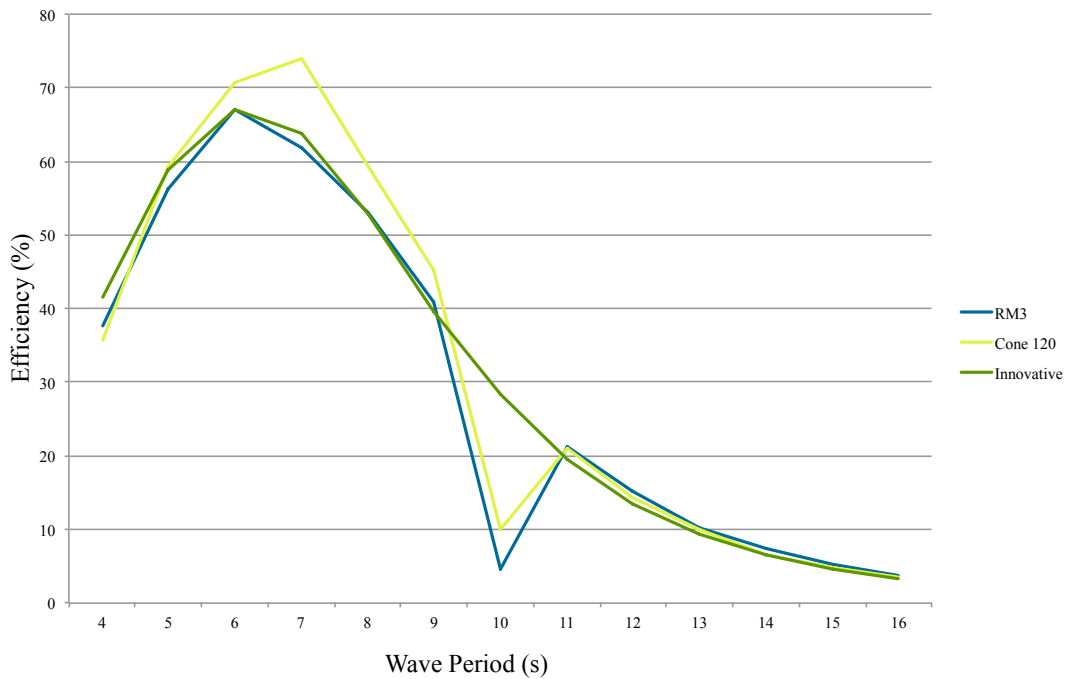for each geometry. Similar to the regular wave results for mass, the efficiency of 120°

Figure 17. Efficiency as a function of wave period for each float design at a mass of 500,000 kg in regular waves
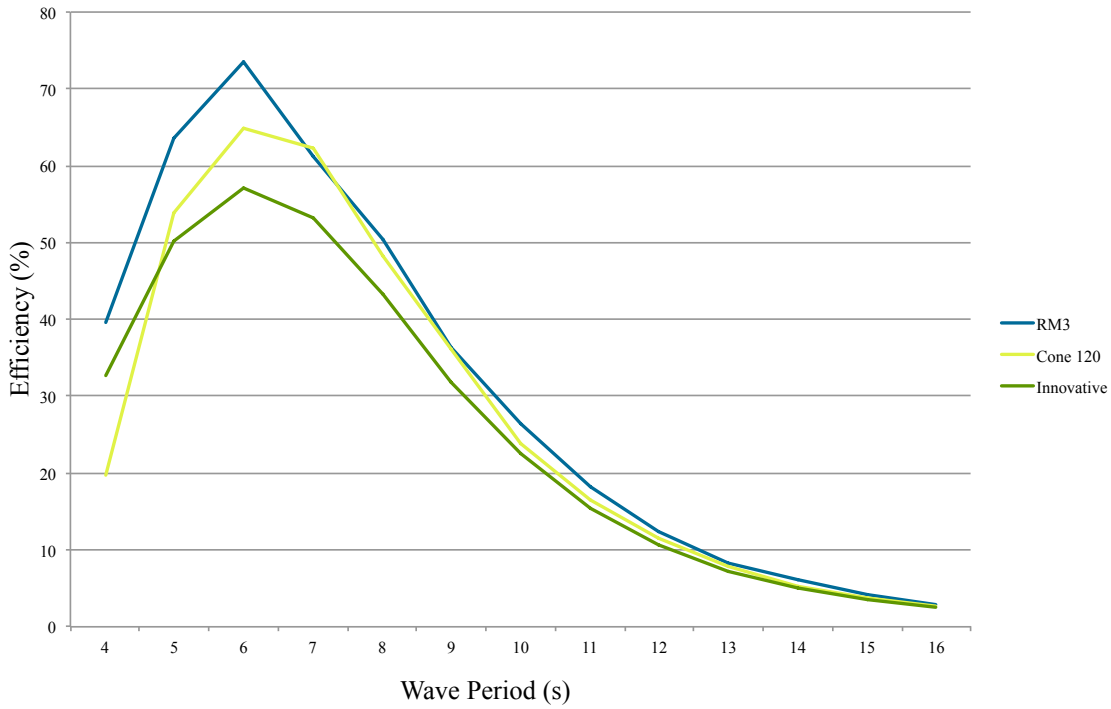
Figure 18. Efficiency as a function of wave period for each float design at a mass of 1,000,000 kg in regular waves
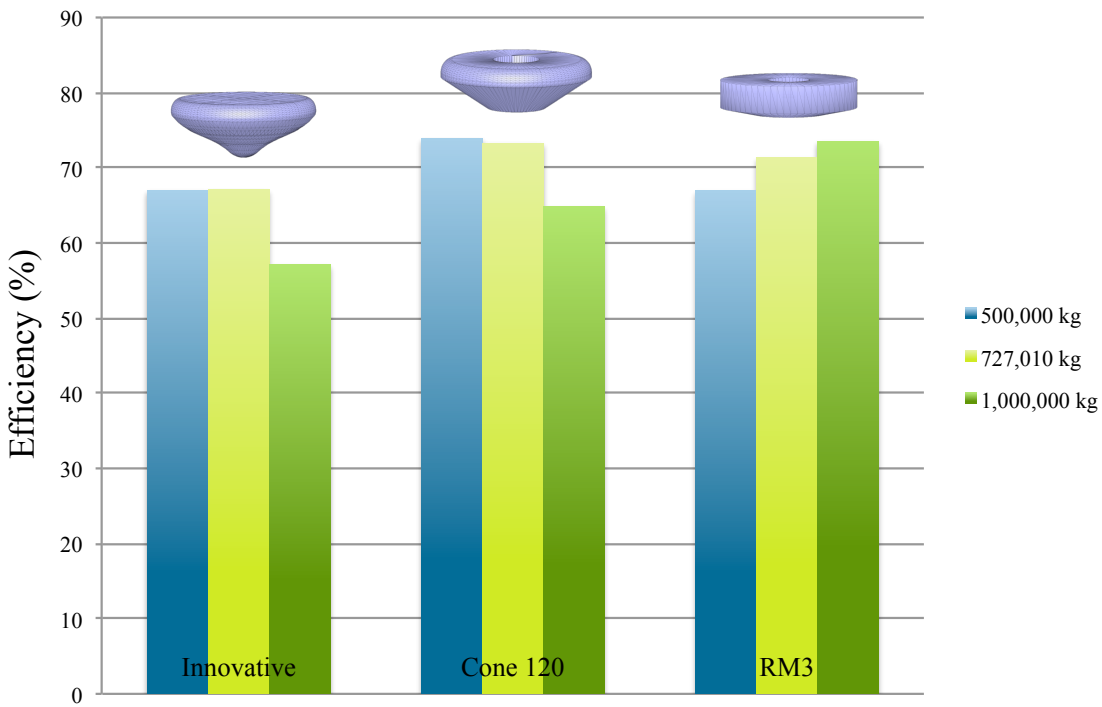

Figure 19. Maximum efficiency for each geometry at each mass for regular waves (At various periods (120° cone at 500,000 kg peak period at 7 seconds, remaining at 6))
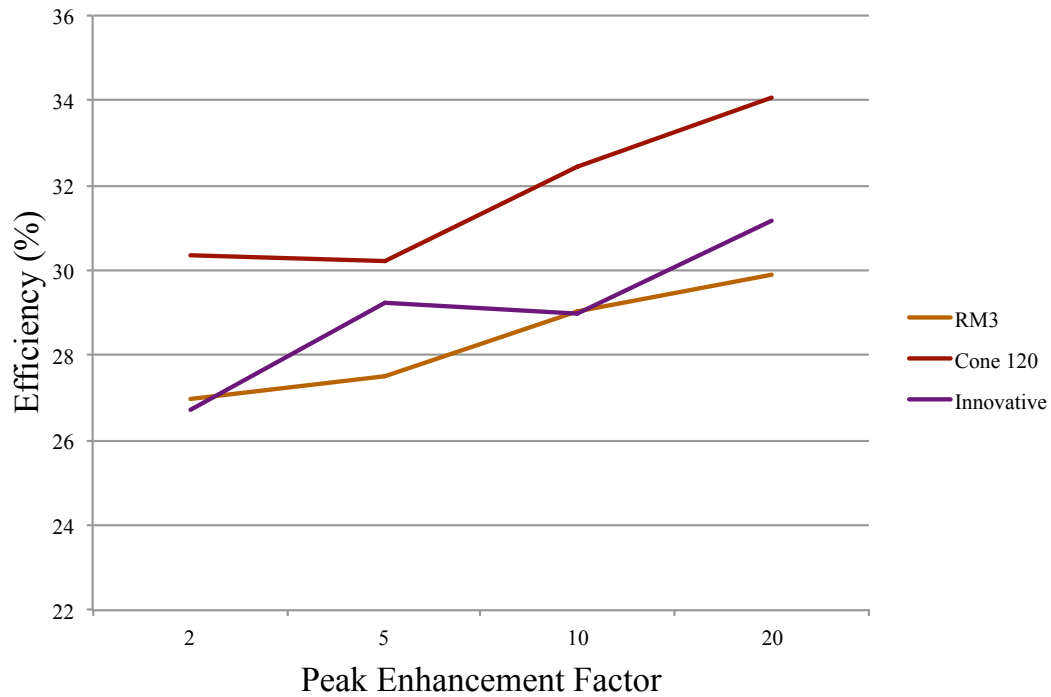
29

Figure 20. Efficiency as a function of peak enhancement factor for each float design at a mass of 500,000 kg in irregular waves
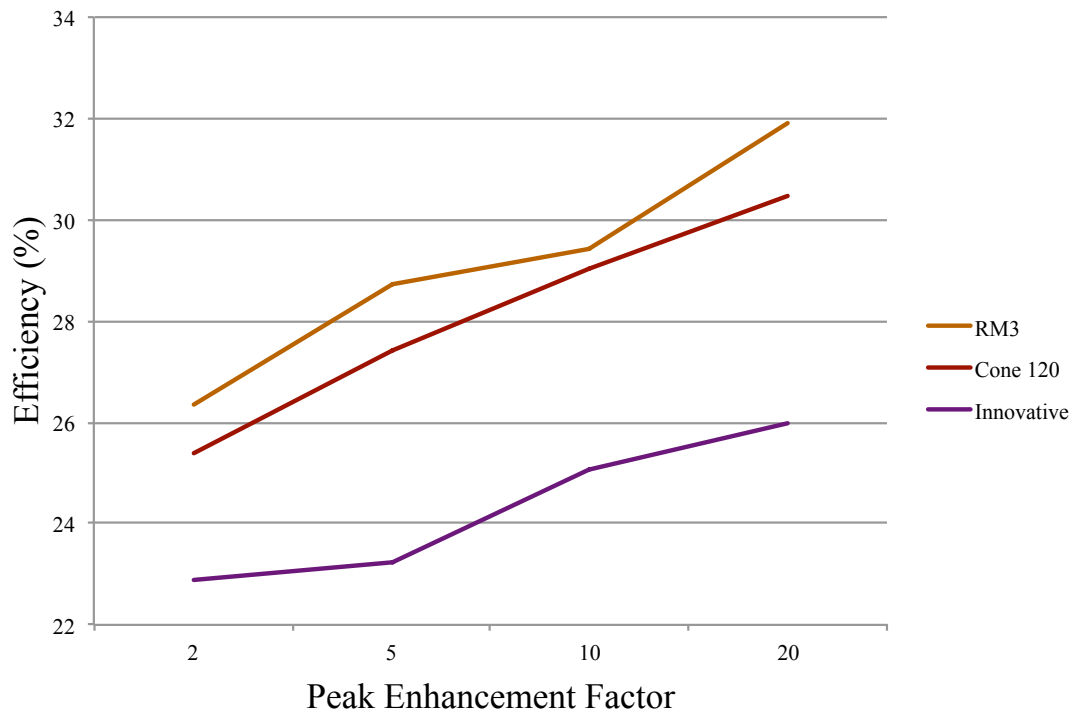

Figure 21. Efficiency as a function of peak enhancement factor for each float design at a mass of 1,000,000 kg in irregular waves
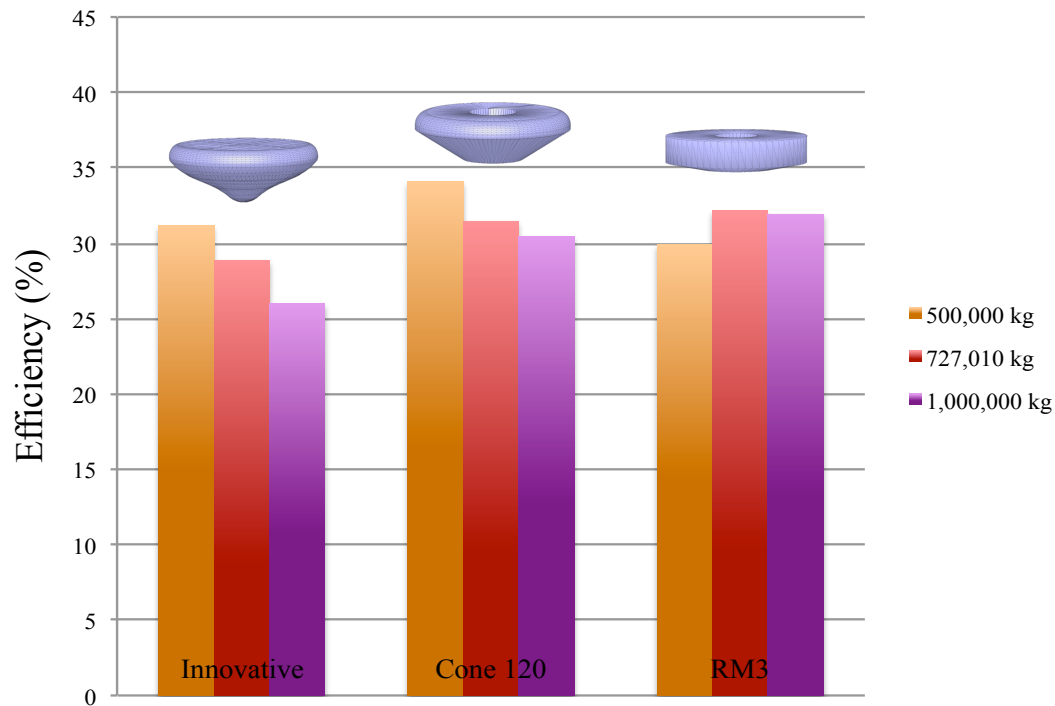
Figure 22. Maximum efficiency for each geometry at each mass for irregular waves (At a peak enhancement factor of 20)

cone and innovative decreased as mass increased and the efficiency of RM3 increased as mass increased. The same implications for mass in regular waves applies to the irregular wave cases, however, the greatest efficiencies overall were of the smaller masses.

For the damping trials, mass was held constant. Figure 23 illustrates the efficiency of each float with a damping coefficient of 2,500 kN/(m/s) as a function of wave period in regular waves. The peak period for each design shifted to the right with an increase in the damping coefficient. Innovative and 120° cone were the most efficient with efficiencies of 70.29% and 73.88%, respectively. Similar to Figure 17, 120° cone and RM3 were inconsistent at a period of 10 seconds and innovative showed a steep decrease at a period of 9 seconds. The curves appear to be broader than the floats with a damping coefficient of 1,200 kN/(m/s), as shown in Figure 14.
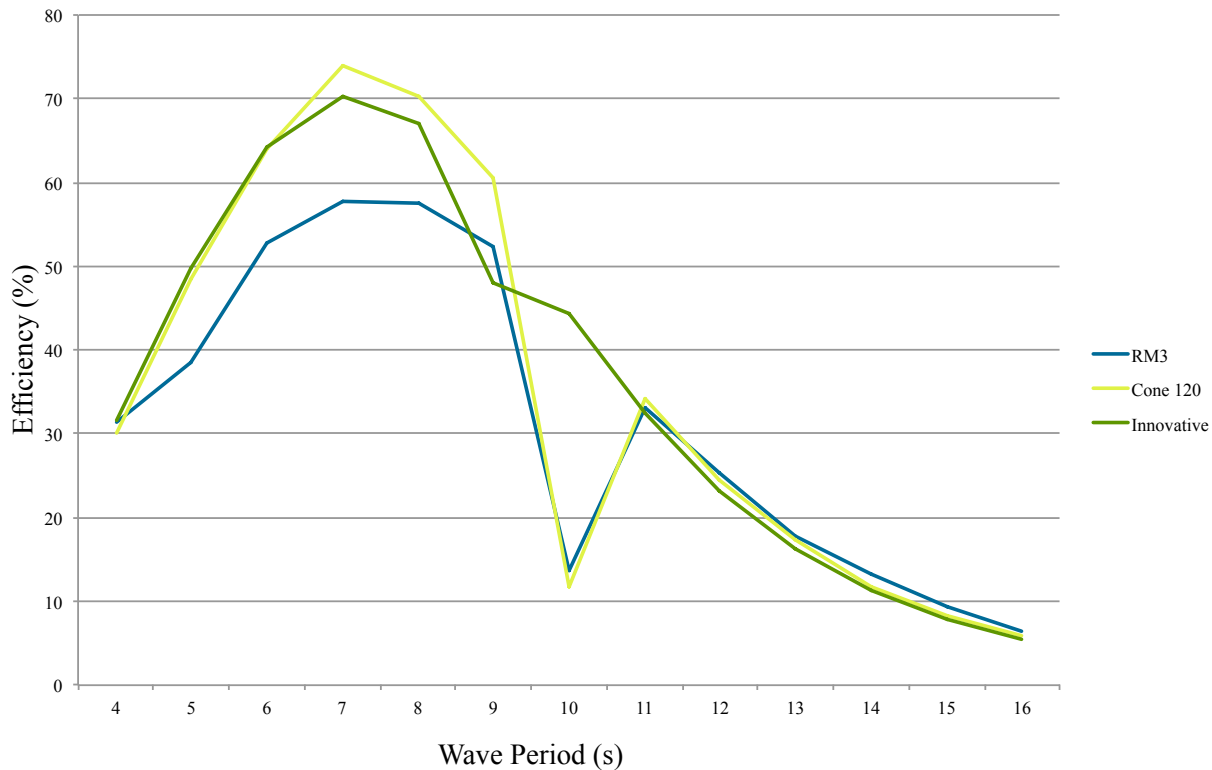
Figure 23. Efficiency as a function of wave period for each float with a damping coefficient of 2,500 kN/(m/s) in regular waves

Figure 24 displays the efficiency as a function of wave period for each float with a damping coefficient of 4,800 kN/(m/s) in regular waves. The curves of these trends would appear to be the broadest when compared to the floats with the smaller damping coefficients, however, the peak efficiencies have decreased, with the most efficient being innovative at an efficiency of 68.56%. The efficiencies of each float drop around 9 to 10 seconds. The inconsistencies appear to be a pattern implying that there is difficulty for the designs to resonate at these periods. Figure 25 illustrates an overview of the damping trials with the maximum efficiency of each float in regular waves shown. For 120° cone and innovative, the maximum efficiency occurred at a damping coefficient of 2,500 kN/(m/s), whereas the maximum efficiency of RM3 was at the default damping coefficient of 1,200 kN/(m/s). The efficiency of RM3 decreases drastically as the damping coefficient increases implying that the default damping would be the
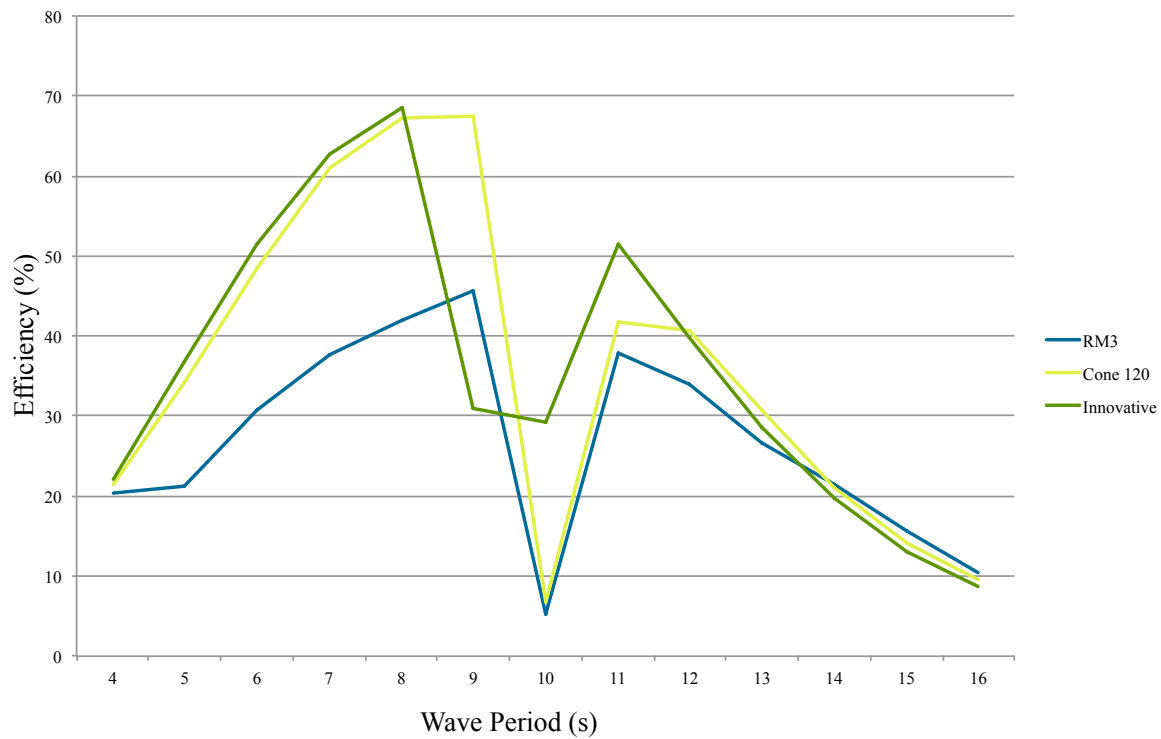
32

Figure 24. Efficiency as a function of wave period for each float with a damping coefficient of 4,800 kN/(m/s) in regular waves
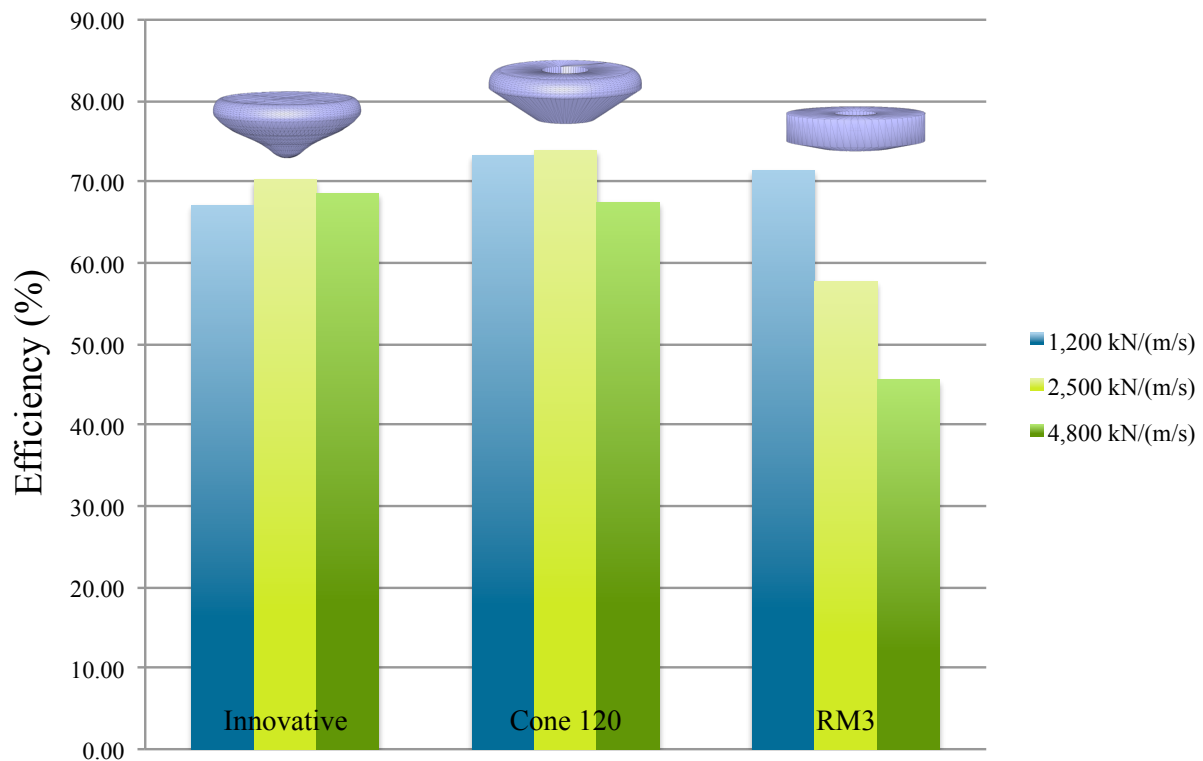

Figure 25. Maximum efficiency for each geometry at each damping coefficient for regular waves (at varying periods. (all floats at 1,200 kN/(m/s) at a period of 6 seconds, all floats at 2,500 kN/(m/s) at a period of 7 seconds; Innovative at 8 seconds, and 120° cone and RM3 at 9 seconds for 4,800 kN/(m/s))

optimal damping design for RM3, whereas the optimal damping for 120° cone and innovative would be at or greater than 2,500 and less than 4,800 kN/(m/s). Similar to the mass trials, the efficiency is a function of both damping and geometry as optimal damping varies with geometry. For irregular waves, Figure 26 and 27 illustrate the efficiency as a function of peak enhancement factor for all floats with a damping coefficient of 2,500 and 4,800 kN/(m/s), respectively. For the damping coefficient of 2,500 kN/(m/s), 120° cone is the most efficient overall with an efficiency of 32.14%, followed by innovative, then RM3. For the damping coefficient of 4,800 kN/(m/s), innovative is the most efficient with an efficiency of 26.58%, followed by 120° cone, then RM3. For the higher damping coefficient, however, the overall efficiency decreased for all floats. This can be seen in Figure 28, as the maximum efficiencies for each float
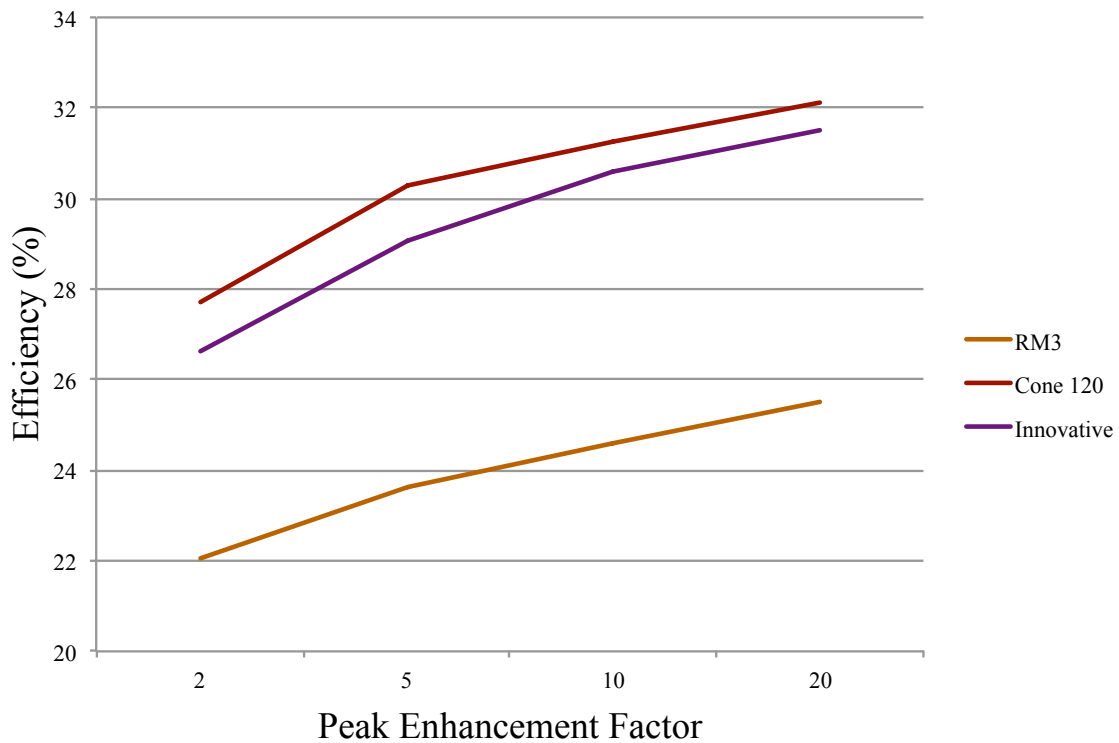

Figure 26. Efficiency as a function of peak enhancement factor for each float design at a damping coefficient of 2,500 kN/(m/s) in irregular waves.
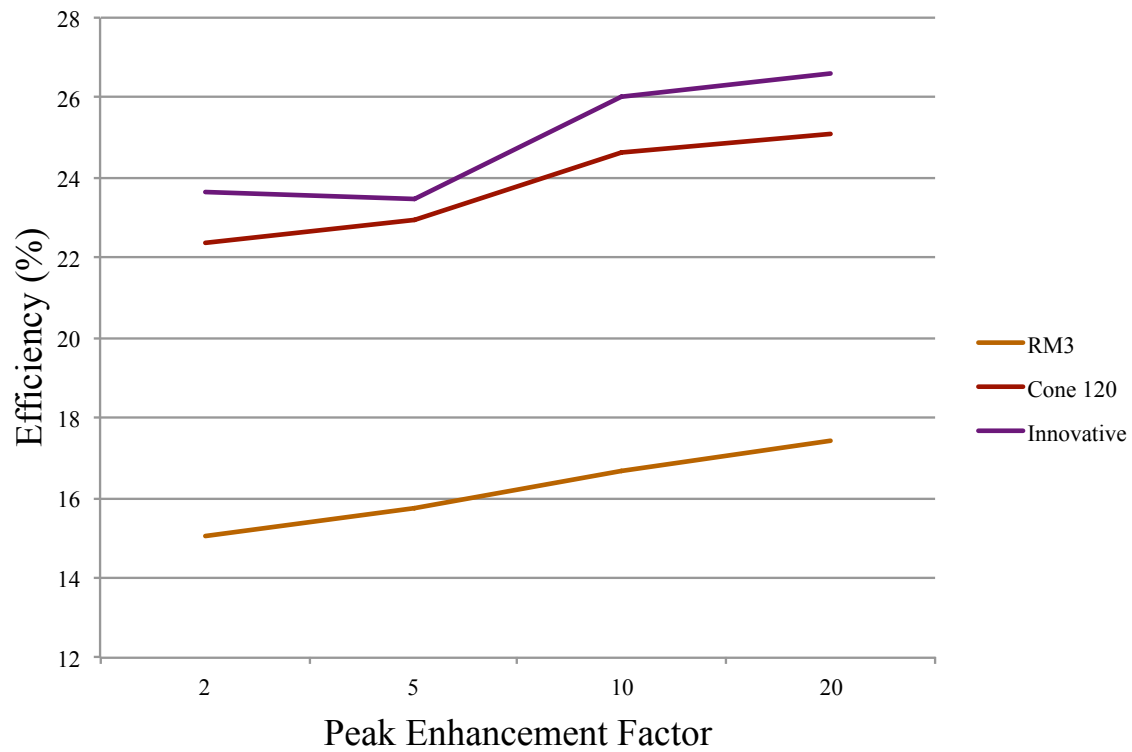
Figure 27. Efficiency as a function of peak enhancement factor for each float design at a damping coefficient of 4,800 kN/(m/s) in irregular waves

and damping coefficient are shown. The maximum efficiency overall was 32.16% with RM3 at 1,200 kN/(m/s), but 120° cone and innovative followed close behind with a damping coefficient of 2,500 kN/(m/s). Similar to the results of damping in regular waves, the optimal damping design for RM3 is 1,200 kN/(m/s), and the optimal damping design for innovative and 120° cone is either at or greater than 2,500 kN/(m/s) and less than 4,800 kN/(m/s). The efficiency also appears to be a function of both damping and geometry as the optimal damping varies with geometry.
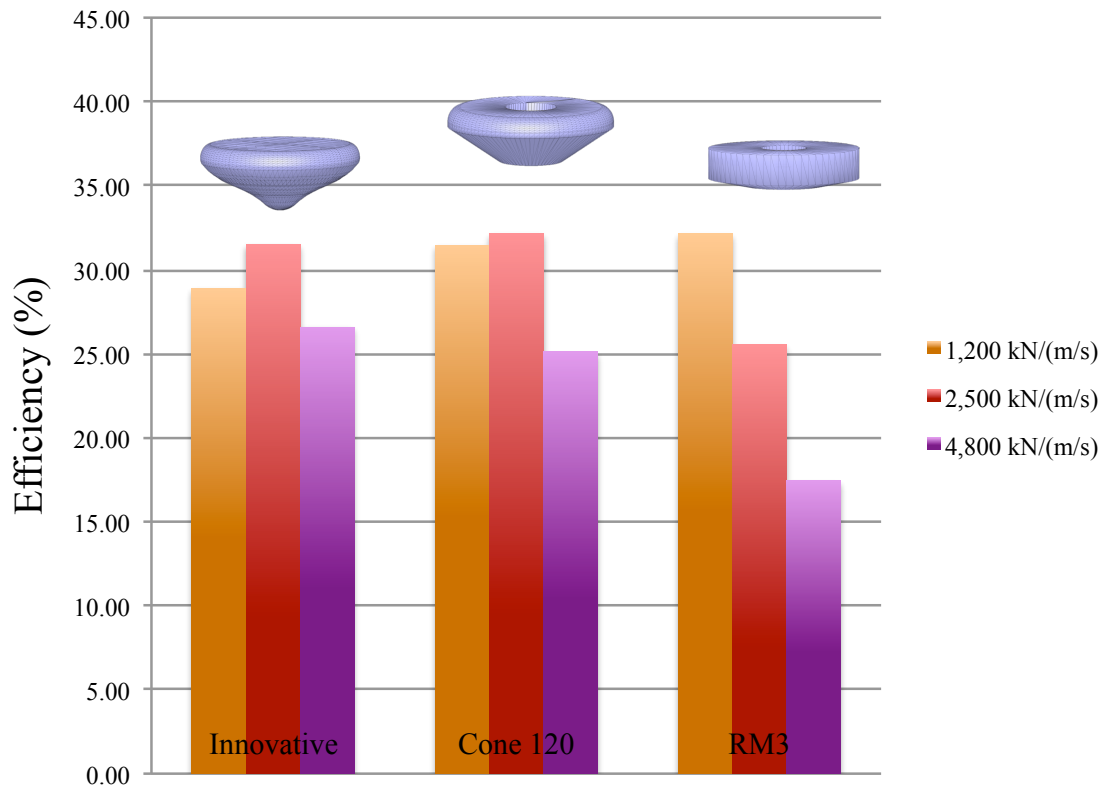
Figure 28. Maximum efficiency for each geometry at each damping coefficient for irregular waves (At a peak enhancement factor of 20)

3.4   STATISTICAL ANALYSIS

For the irregular wave trials, efficiency varied because not every realization of the wave spectrum is identical, so the float, though the same, will respond differently. With 95% confidence, the efficiency maintained a relatively small variation, showing consistency in its values. As the peak enhancement factor increases, however, the variation decreases as this accounts for the decrease in variation of the waves. Figure 29 illustrates the confidence interval on each set of trials for efficiency as a function of peak enhancement factor for each geometry with a mass of 727,010 kg and a damping coefficient of 1,200 kN/(m/s).
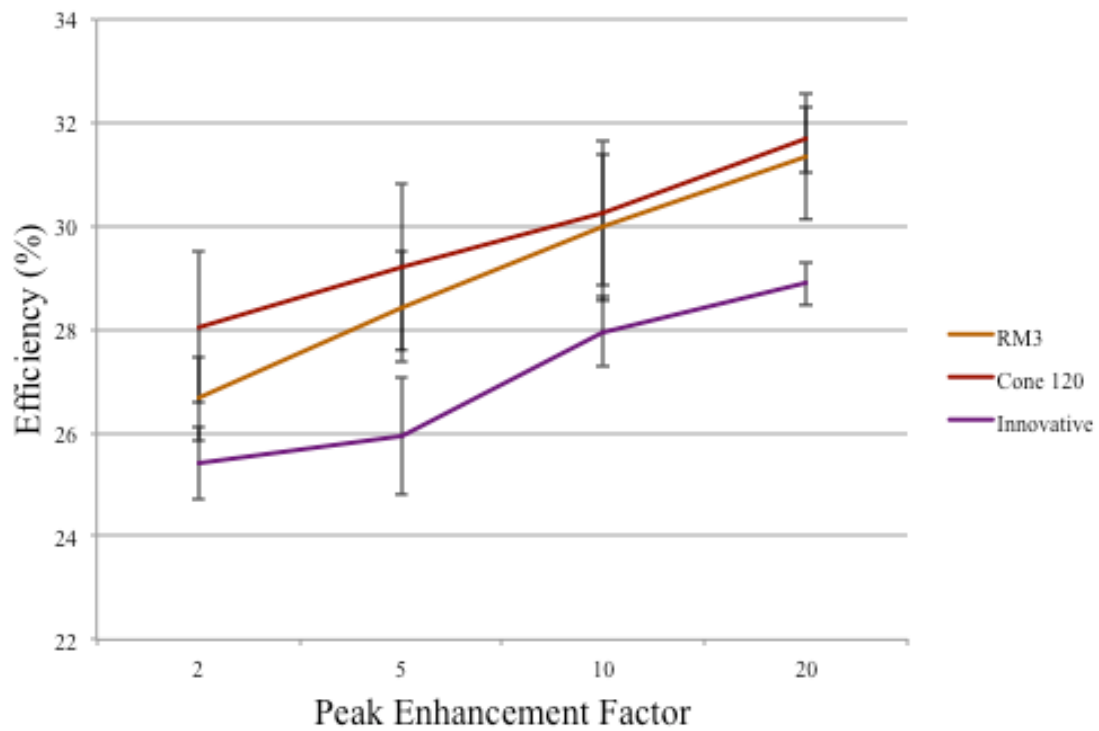
Figure 29. Efficiency as a function of peak enhancement factor for each geometry with mass of 727,010 kg and damping coefficient of 1,200 kN/(m/s)

CHAPTER 4

CONCLUSION

To conclude, geometry, mass, and damping are certainly considerable factors in designing point absorber floats, however, efficient energy conversion in irregular waves remains a challenge. From this study, differing results were obtained in comparison to literature and a new approach in design was tested. Banasiak et al. (2004) concluded in their study that the hemispherical and 90° conical float designs were the most efficient, whereas this study concludes that the 120° conical float is the most efficient overall. The innovative float design was slightly less efficient than that of the 120° cone, and in some cases, was more efficient than RM3. Because the innovative float was designed solely based off the irregular wave analysis with a similar capture width to RM3 and that it competed with the most efficient designs, shows that there is merit to the design approach.

Concerning mass and damping, both vary optimally for each of the three geometries tested. For two of the three floats tested, an increase in the damping coefficient allowed a broadening of the efficiency curve. Though in these cases the peak efficiency decreases, it may be more beneficial to increase the damping coefficient in order to collect the maximum amount of energy over time. In comparing the three floats tested in Phase II, all had very similar geometries. The wetted surfaces of each float have a gentle slope from the horizontal. It can be concluded that this particular design may lead to the optimization of float geometry. Concerning resonance, however, the results

study lacks implications and relationships between the properties of the float and resonance.

The results of this study imply that mass and damping should be optimized for each individual float design and that openness to creativity and unconventionality can lead to interesting results. Considering the hydrodynamics of irregular waves and the commonalities between each unique wave could introduce new ways to approach the geometric design as well as other design factors of point absorbers.

Limitations include the possibility of inaccuracy in modeling and restricted knowledge and resources. The functionality and simulations of WEC-Sim have been compared to codes such as WaveDyn, AQWA, and OrcaFlex, as well as the data from an experimental wave tank (Ruehl, 2014). The results from these experiments validate the ability of WEC-Sim to reproduce experimental results, however, there is a possibility of the predictions being inaccurate. Lack of knowledge and resources revealing the relationship of inertial forces, added mass, and resonance proved difficult in designing the innovative float. Simply mirroring the appearance of a pattern in irregular waves and following intuition, though relatively effective, lacks mathematical basis that could potentially lead to a more effective design. Additionally, an understanding of capture width prior to the experiment would have allowed more effective results. Each float varied slightly by capture width, which affected how efficiency responded to the changes in dependent variables. A more accurate experiment, in mass for example, would involve the floats with the same capture width, volume, and mass, but varying geometries and centers of mass. Instead, the floats were resized until the masses and volumes were approximately equal, varying the capture width.

In continuing this work, studying the geometries with constant capture widths could improve results and possibly provide new insights. Also, floats could be designed specifically for certain wave spectrums. The innovative float was designed specifically for a peak period of 6.5 seconds and a significant wave height of 2.5m and proved to be efficient, so other floats could be designed using similar methods for areas with larger waves and longer peak periods. Lastly, the innovative float was designed based off the angles of the resultant force distribution, but the float could also be designed based off the magnitude of each resultant force in the distribution. This would involve concepts of inertia and solving for equations that optimize either the radius of gyration or distribution of mass. Exploring this approach could lead to more effective designs for the floats of point absorbers.

REFERENCES

Antonio, Falcão D. O. (2010). Wave energy utilization: A review of the technologies. Renewable and sustainable energy reviews, 14(3), 899-918.

Babarit, A., Delhommeau, G. (2015). Theoretical and numerical aspects of the open source BEM solver NEMOH. In Proc. of the 11th European Wave and Tidal Energy Conference, Nantes, France

Babarit, A., Hals, J., Muliawan, M. J., Kurniawan, A., Moan, T., & Krokstad, J. (2012). Numerical benchmarking study of a selection of wave energy converters. Renewable Energy, 41, 44-63.

Banasiak, R., Vantorre, M., Verhoeven, R. (2004). Modelling of hydraulic performance and wave energy extraction by a point absorber in heave. Applied Ocean Research, 26(2004), 61-72.

Lee, C.H., Newman, J.H. (2006). WAMIT User Manual.

López, I., Andreu, J., Ceballos, S., de Alegría, I. M., & Kortabarria, I. (2013). Review of wave energy technologies and the necessary power-equipment. Renewable and Sustainable Energy Reviews, 27, 413-434.

Li, Y., & Yu, Y. H. (2012). A synthesis of numerical methods for modeling wave energy

    converter-point absorbers. Renewable and Sustainable Energy Reviews, 16(6),

    4352-4364.

Neary, V. S., Lawson, M., Previsic, M., Copping, A., Hallett, K. C., Labonte, A., ... &

    Murray, D. (2014). Methodology for design and economic analysis of marine

    energy conversion (MEC) technologies.

Ruehl, K., Michelen, C., Kanner, S., Lawson, M., & Yu, Y. H. (2014, June). Preliminary

    verification and validation of WEC-Sim, an open-source wave energy converter

    design tool. In 33rd International Conference on Ocean, Offshore and Arctic

    Engineering, OMAE, San Francisco, CA, United States (Abstract accepted).

Salter, S. H. (1974). Wave power. Nature, 249(5459), 720-724.

Y. Yu, M. Lawson, K. Ruehl, and C. Michelen, "Development and Demonstration of the

    WEC-Sim Wave Energy Converter Simulation Tool," in Proceedings of the 2nd

    Marine Energy Technology Symposium, Seattle, WA, 2014.